

Differential Flatness of Quadrotor Dynamics Subject to Rotor Drag for Accurate Tracking of High-Speed Trajectories

Matthias Faessler, Antonio Franchi, Davide Scaramuzza

▶ **To cite this version:**

Matthias Faessler, Antonio Franchi, Davide Scaramuzza. Differential Flatness of Quadrotor Dynamics Subject to Rotor Drag for Accurate Tracking of High-Speed Trajectories. IEEE Robotics and Automation Letters, 2018, 3 (2), pp.620-626. hal-01658577v2

HAL Id: hal-01658577

https://laas.hal.science/hal-01658577v2

Submitted on 14 Dec 2017

HAL is a multi-disciplinary open access archive for the deposit and dissemination of scientific research documents, whether they are published or not. The documents may come from teaching and research institutions in France or abroad, or from public or private research centers.

L'archive ouverte pluridisciplinaire **HAL**, est destinée au dépôt et à la diffusion de documents scientifiques de niveau recherche, publiés ou non, émanant des établissements d'enseignement et de recherche français ou étrangers, des laboratoires publics ou privés.

Preprint version, final version at http://ieeexplore.ieee.org/ accepted for IEEE Robotics and Automation Letters (RA-L) 2018

Differential Flatness of Quadrotor Dynamics Subject to Rotor Drag for Accurate Tracking of High-Speed Trajectories

Matthias Faessler[1], Antonio Franchi[2], and Davide Scaramuzza[1]

***Abstract*— In this paper, we prove that the dynamical model of a quadrotor subject to linear rotor drag effects is differentially flat in its position and heading. We use this property to compute feed-forward control terms directly from a reference trajectory to be tracked. The obtained feed-forward terms are then used in a cascaded, nonlinear feedback control law that enables accurate agile flight with quadrotors. Compared to state-of-the-art control methods, which treat the rotor drag as an unknown disturbance, our method reduces the trajectory tracking error significantly. Finally, we present a method based on a gradient-free optimization to identify the rotor drag coefficients, which are required to compute the feed-forward control terms. The new theoretical results are thoroughly validated trough extensive comparative experiments.**

Supplementary Material

Video of the experiments: `https://youtu.be/VIQILwcM5PA`

I. Introduction

A. Motivation

For several years, quadrotors have proven to be suitable aerial platforms for performing agile flight maneuvers . Nevertheless, quadrotors are typically controlled by neglecting aerodynamic effects, such as rotor drag, that only become important for non-hover conditions. These aerodynamic effects are treated as unknown disturbances, which works well when controlling the quadrotor close to hover conditions but reduces its trajectory tracking accuracy progressively with increasing speed. For fast obstacle avoidance it is important to perform accurate agile trajectory tracking. To achieve this, we require a method for accurate tracking of trajectories that are unknown prior to flying.

The main aerodynamic effect causing trajectory tracking errors during high-speed flight is rotor drag, which is a linear effect in the quadrotor's velocity [1]. In this work, we aim at developing a control method that improves the trajectory tracking performance of quadrotors by considering the rotor drag effect. To achieve this, we first prove that the dynamical model of a quadrotor subject to linear rotor drag effects is differentially flat with flat outputs chosen to be its position and heading. We then use this property to compute feed-forward control terms directly from the reference trajectory to be tracked. The obtained feed-forward terms are then used in a cascaded, nonlinear feedback control law that enables accurate agile flight with quadrotors on a priori unknown trajectories. Finally, we present a method based on a gradient-free optimization to identify the rotor drag coefficients which are required to compute the feed-forward control terms. We validate our theoretical results through experiments with a quadrotor shown in Fig. 1.

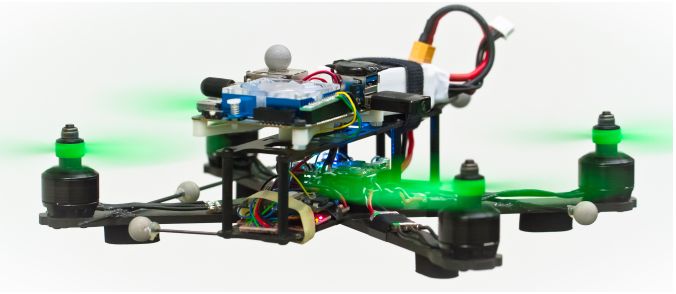


Fig. 1: First-person-view racing inspired quadrotor platform used for the presented experiments.

B. Related Work

In [2], it was shown that the common model of a quadrotor *without* considering rotor drag effects is differentially flat when choosing its position and heading as flat outputs. Furthermore, this work presented a control algorithm that computes the desired collective thrust and torque inputs from the measured position, velocity, orientation, and body-rates errors. With this method, agile maneuvers with speeds of several meters per second were achieved. In [3], the differential flatness property of a hexarotor that takes the desired collective thrust and its desired orientation as inputs was exploited to compute feed-forward terms used in an LQR feedback controller. The desired orientation was then controlled by a separate low-level control loop, which also enables the execution of flight maneuvers with speeds of several meters per second. We extend these works by showing that the dynamics of a quadrotor are differentially flat even when they are subject to linear rotor drag effects. Similarly to [3], we make use of this property to compute feed-forward terms that are then applied by a position controller.

Rotor drag effects influencing a quadrotor's dynamics were investigated in [4] and [5] where also a control law was presented, which considers these dynamics. Rotor drag effects originate from blade flapping and induced drag of the rotors, which are, thanks to their equivalent mathematical

This research was supported by the National Centre of Competence in Research (NCCR) Robotics, the SNSF-ERC Starting Grant, the DARPA FLA program, and the European Union's Horizon 2020 research and innovation program under grant agreement No 644271 AEROARMS.

[1]The two authors are with the Robotics and Perception Group, Dep. of Informatics University of Zurich and Dep. of Neuroinformatics of the University of Zurich and ETH Zurich, Switzerland—`http://rpg.ifi.uzh.ch`.

[2]Antonio Franchi is with LAAS-CNRS, Université de Toulouse, CNRS, Toulouse, France.

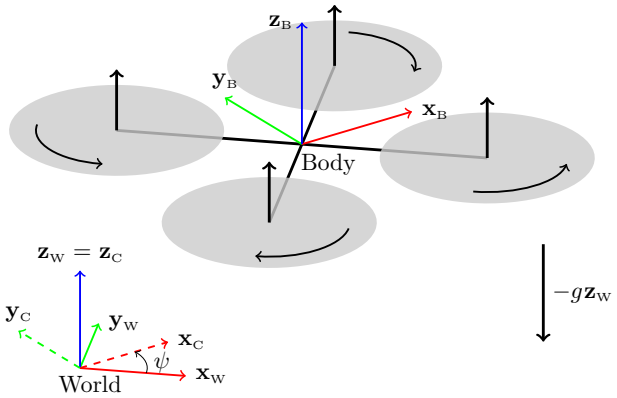


Fig. 2: Schematics of the considered quadrotor model with the used coordinate systems.

expression, typically combined as linear effects in a lumped parameter dynamical model [6]. These rotor drag effects were then incorporated in dynamical models of multi rotors to improve state estimation in [7] and [8]. In this work, we make use of the fact that the main aerodynamic effects are of similar nature and can therefore be described together by lumped parameters in a dynamical model.

In [9], the authors achieve accurate thrust control by electronic speed controllers through a model of the aerodynamic power generated by a fixed-pitch rotor under wind disturbances, which reduces the trajectory tracking error of a quadrotor. Rotor drag was also considered in control methods for multi-rotor vehicles in [10] and [11], where the control problem was simplified by decomposing the rotor drag force into a component that is independent of the vehicle's orientation and one along the thrust direction, which leads to an explicit expression for the desired thrust direction. In [13], a refined thrust model and a control scheme that considers rotor drag in the computation of the thrust command and the desired orientation are presented. Additionally to the thrust command and desired orientation, the control scheme in [14] also computes the desired body rates and angular accelerations by considering rotor drag but requires estimates of the quadrotor's acceleration and jerk, which are usually not available. In contrast, we compute the exact reference thrust, orientation, body rates, and angular accelerations considering rotor drag only from a reference trajectory, which we then use as feed-forward terms in the controller.

II. Nomenclature

In this work, we make use of a world frame W with orthonormal basis $\{\mathbf{x}_\mathrm{W}, \mathbf{y}_\mathrm{W}, \mathbf{z}_\mathrm{W}\}$ represented in world coordinates and a body frame B with orthonormal basis $\{\mathbf{x}_\mathrm{B}, \mathbf{y}_\mathrm{B}, \mathbf{z}_\mathrm{B}\}$ also represented in world coordinates. The body frame is fixed to the quadrotor with an origin coinciding with its center of mass as depicted in Fig. 2. The quadrotor is subject to a gravitational acceleration g in the $-\mathbf{z}_\mathrm{W}$ direction. We denote the position of the quadrotor's center of mass as $\mathbf{p}$, and its derivatives, velocity, acceleration, jerk, and snap as $\mathbf{v}$, $\mathbf{a}$, $\mathbf{j}$, and $\mathbf{s}$, respectively. We represent the quadrotor's orientation as a rotation matrix $\mathbf{R} = \begin{bmatrix}\mathbf{x}_\mathrm{B} & \mathbf{y}_\mathrm{B} & \mathbf{z}_\mathrm{B}\end{bmatrix}$ and its body rates (i.e., the angular velocity) as $\boldsymbol{\omega}$ represented in body coordinates. To denote a unit vector along the z-coordinate axis we write $\mathbf{e}_z$. Finally, we denote quantities that can be computed from a reference trajectory as *reference values* and quantities that are computed by an outer loop feedback control law and passed to an inner loop controller as *desired values*.

III. Model

We consider the dynamical model of a quadrotor with rotor drag developed in [10] with no wind, stiff propellers, and no dependence of the rotor drag on the thrust. According to this model, the dynamics of the position $\mathbf{p}$, velocity $\mathbf{v}$, orientation $\mathbf{R}$, and body rates $\boldsymbol{\omega}$ can be written as

$$\dot{\mathbf{p}} = \mathbf{v} \tag{1}$$

$$\dot{\mathbf{v}} = -g\mathbf{z}_\mathrm{W} + c\mathbf{z}_\mathrm{B} - \mathbf{R}\mathbf{D}\mathbf{R}^\top\mathbf{v} \tag{2}$$

$$\dot{\mathbf{R}} = \mathbf{R}\hat{\boldsymbol{\omega}} \tag{3}$$

$$\dot{\boldsymbol{\omega}} = \mathbf{J}^{-1}\left(\boldsymbol{\tau} - \boldsymbol{\omega}\times\mathbf{J}\boldsymbol{\omega} - \boldsymbol{\tau}_\mathrm{g} - \mathbf{A}\mathbf{R}^\top\mathbf{v} - \mathbf{B}\boldsymbol{\omega}\right) \tag{4}$$

where c is the mass-normalized collective thrust, $\mathbf{D} = \mathrm{diag}\left(d_x, d_y, d_z\right)$ is a constant diagonal matrix formed by the mass-normalized rotor-drag coefficients, $\hat{\boldsymbol{\omega}}$ is a skew-symmetric matrix formed from $\boldsymbol{\omega}$, $\mathbf{J}$ is the quadrotor's inertia matrix, $\boldsymbol{\tau}$ is the three dimensional torque input, $\boldsymbol{\tau}_\mathrm{g}$ are gyroscopic torques from the propellers, and $\mathbf{A}$ and $\mathbf{B}$ are constant matrices. For the derivations and more details about these terms, please refer to [10]. In this work, we adopt the thrust model presented in [13]

$$c = c_\mathrm{cmd} + k_h v_h^2 \tag{5}$$

where c_cmd is the commanded collective thrust input, k_h is a constant, and $v_h = \mathbf{v}^\top(\mathbf{x}_\mathrm{B} + \mathbf{y}_\mathrm{B})$. The term $k_h v_h^2$ acts as a quadratic velocity-dependent input disturbance which adds up to the input c_cmd. The additional linear velocity-dependent disturbance in the $\mathbf{z}_\mathrm{B}$ direction of the thrust model in [13] is lumped by d_z directly in (2) by neglecting its dependency on the rotor speeds. Note that this dynamical model of a quadrotor is a generalization of the common model found, e.g., in [2], in which the linear rotor drag components are typically neglected, i.e., $\mathbf{D}$, $\mathbf{A}$ and $\mathbf{B}$ are considered null matrices.

IV. Differential Flatness

In this section, we show that the extended dynamical model of a quadrotor subject to rotor drag (1)-(4) with four inputs is differentially flat, like the model with neglected drag [2]. In fact, we shall show that the states $[\mathbf{p}, \mathbf{v}, \mathbf{R}, \boldsymbol{\omega}]$ and the inputs $[c_\mathrm{cmd}, \boldsymbol{\tau}]$ can be written as algebraic functions of four selected flat outputs and a finite number of their derivatives. Equally to [2], we choose the flat outputs to be the quadrotor's position $\mathbf{p}$ and its heading ψ.

To show that the orientation $\mathbf{R}$ and the collective thrust c are functions of the flat outputs, we reformulate (2) as

$$\begin{aligned} c\mathbf{z}_\mathrm{B} - \left(d_x\mathbf{x}_\mathrm{B}^\top\mathbf{v}\right)\mathbf{x}_\mathrm{B} - \left(d_y\mathbf{y}_\mathrm{B}^\top\mathbf{v}\right)\mathbf{y}_\mathrm{B} - \left(d_z\mathbf{z}_\mathrm{B}^\top\mathbf{v}\right)\mathbf{z}_\mathrm{B} \\ - \mathbf{a} - g\mathbf{z}_\mathrm{W} = 0. \end{aligned} \tag{6}$$

From left-multiplying (6) by $\mathbf{x}_\mathrm{B}^\top$ we get

$$\mathbf{x}_\mathrm{B}^\top \boldsymbol{\alpha} = 0, \text{ with } \quad \boldsymbol{\alpha} = \mathbf{a} + g\mathbf{z}_\mathrm{W} + d_x \mathbf{v}. \tag{7}$$

From left-multiplying (6) by $\mathbf{y}_\mathrm{B}^\top$ we get

$$\mathbf{y}_\mathrm{B}^\top \boldsymbol{\beta} = 0, \text{ with } \quad \boldsymbol{\beta} = \mathbf{a} + g\mathbf{z}_\mathrm{W} + d_y \mathbf{v}. \tag{8}$$

To enforce a reference heading ψ, we constrain the projection of the $\mathbf{x}_\mathrm{B}$ axis into the $\mathbf{x}_\mathrm{W} - \mathbf{y}_\mathrm{W}$ plane to be collinear with $\mathbf{x}_\mathrm{C}$ (cf. Fig. 2), where

$$\mathbf{x}_\mathrm{C} = \begin{bmatrix} \cos(\psi) & \sin(\psi) & 0 \end{bmatrix}^\top \tag{9}$$

$$\mathbf{y}_\mathrm{C} = \begin{bmatrix} -\sin(\psi) & \cos(\psi) & 0 \end{bmatrix}^\top. \tag{10}$$

From this, (7) and (8), and the constraints that $\mathbf{x}_\mathrm{B}$, $\mathbf{y}_\mathrm{B}$, and $\mathbf{z}_\mathrm{B}$ must be orthogonal to each other and of unit length, we can construct $\mathbf{R}$ with

$$\mathbf{x}_\mathrm{B} = \frac{\mathbf{y}_\mathrm{C} \times \boldsymbol{\alpha}}{\|\mathbf{y}_\mathrm{C} \times \boldsymbol{\alpha}\|} \tag{11}$$

$$\mathbf{y}_\mathrm{B} = \frac{\boldsymbol{\beta} \times \mathbf{x}_\mathrm{B}}{\|\boldsymbol{\beta} \times \mathbf{x}_\mathrm{B}\|} \tag{12}$$

$$\mathbf{z}_\mathrm{B} = \mathbf{x}_\mathrm{B} \times \mathbf{y}_\mathrm{B}. \tag{13}$$

One can verify that these vectors are of unit length, perpendicular to each other, and satisfy the constraints (7) - (10). To get the collective thrust, we left-multiply (6) by $\mathbf{z}_\mathrm{B}^\top$

$$c = \mathbf{z}_\mathrm{B}^\top \left(\mathbf{a} + g\mathbf{z}_\mathrm{W} + d_z \mathbf{v}\right). \tag{14}$$

Then the collective thrust input can be computed as a function of c, $\mathbf{R}$, and the flat outputs, as

$$c_\mathrm{cmd} = c - k_h(\mathbf{v}^\top(\mathbf{x}_\mathrm{B} + \mathbf{y}_\mathrm{B}))^2. \tag{15}$$

To show that the body rates $\boldsymbol{\omega}$ are functions of the flat outputs and their derivatives, we take the derivative of (2)

$$\mathbf{j} = \dot{c}\mathbf{z}_\mathrm{B} + c\mathbf{R}\hat{\boldsymbol{\omega}}\mathbf{e}_z - \mathbf{R}\left(\left(\hat{\boldsymbol{\omega}}\mathbf{D} + \mathbf{D}\hat{\boldsymbol{\omega}}^\top\right)\mathbf{R}^\top\mathbf{v} + \mathbf{D}\mathbf{R}^\top\mathbf{a}\right). \tag{16}$$

Left-multiplying (16) by $\mathbf{x}_\mathrm{B}^\top$ and rearranging terms, we get

$$\begin{aligned} &\omega_y \left(c - \left(d_z - d_x\right)\left(\mathbf{z}_\mathrm{B}^\top\mathbf{v}\right)\right) - \omega_z \left(d_x - d_y\right)\left(\mathbf{y}_\mathrm{B}^\top\mathbf{v}\right) \\ &\quad = \mathbf{x}_\mathrm{B}^\top\mathbf{j} + d_x\mathbf{x}_\mathrm{B}^\top\mathbf{a}. \end{aligned} \tag{17}$$

Left-multiplying (16) by $\mathbf{y}_\mathrm{B}^\top$ and rearranging terms, we get

$$\begin{aligned} &\omega_x \left(c + \left(d_y - d_z\right)\left(\mathbf{z}_\mathrm{B}^\top\mathbf{v}\right)\right) + \omega_z \left(d_x - d_y\right)\left(\mathbf{x}_\mathrm{B}^\top\mathbf{v}\right) \\ &\quad = -\mathbf{y}_\mathrm{B}^\top\mathbf{j} - d_y\mathbf{y}_\mathrm{B}^\top\mathbf{a}. \end{aligned} \tag{18}$$

To get a third constraint for the body rates, we project (3) along $\mathbf{y}_\mathrm{B}$

$$\omega_z = \mathbf{y}_\mathrm{B}^\top\dot{\mathbf{x}}_\mathrm{B}. \tag{19}$$

Since $\mathbf{x}_\mathrm{B}$ is perpendicular to $\mathbf{y}_\mathrm{C}$ and $\mathbf{z}_\mathrm{B}$, we can write

$$\mathbf{x}_\mathrm{B} = \frac{\tilde{\mathbf{x}}_\mathrm{B}}{\|\tilde{\mathbf{x}}_\mathrm{B}\|}, \text{ with } \quad \tilde{\mathbf{x}}_\mathrm{B} = \mathbf{y}_\mathrm{C} \times \mathbf{z}_\mathrm{B}. \tag{20}$$

Taking its derivative as the general derivative of a normalized vector, we get

$$\dot{\mathbf{x}}_\mathrm{B} = \frac{\dot{\tilde{\mathbf{x}}}_\mathrm{B}}{\|\tilde{\mathbf{x}}_\mathrm{B}\|} - \tilde{\mathbf{x}}_\mathrm{B}\frac{\tilde{\mathbf{x}}_\mathrm{B}^\top\dot{\tilde{\mathbf{x}}}_\mathrm{B}}{\|\tilde{\mathbf{x}}_\mathrm{B}\|^3} \tag{21}$$

and, since $\tilde{\mathbf{x}}_\mathrm{B}$ is collinear to $\mathbf{x}_\mathrm{B}$ and therefore perpendicular to $\mathbf{y}_\mathrm{B}$, we can write (19) as

$$\omega_z = \mathbf{y}_\mathrm{B}^\top\frac{\dot{\tilde{\mathbf{x}}}_\mathrm{B}}{\|\tilde{\mathbf{x}}_\mathrm{B}\|}. \tag{22}$$

The derivative of $\tilde{\mathbf{x}}_\mathrm{B}$ can be computed as

$$\dot{\tilde{\mathbf{x}}}_\mathrm{B} = \dot{\mathbf{y}}_\mathrm{C} \times \mathbf{z}_\mathrm{B} + \mathbf{y}_\mathrm{C} \times \dot{\mathbf{z}}_\mathrm{B}, \tag{23}$$

$$= \left(-\dot{\psi}\mathbf{x}_\mathrm{C}\right) \times \mathbf{z}_\mathrm{B} + \mathbf{y}_\mathrm{C} \times \left(\omega_y\mathbf{x}_\mathrm{B} - \omega_x\mathbf{y}_\mathrm{B}\right). \tag{24}$$

From this, (20), (22), and the vector triple product $\mathbf{a}^\top(\mathbf{b} \times \mathbf{c}) = -\mathbf{b}^\top(\mathbf{a} \times \mathbf{c})$ we then get

$$\omega_z = \frac{1}{\|\mathbf{y}_\mathrm{C} \times \mathbf{z}_\mathrm{B}\|}\left(\dot{\psi}\mathbf{x}_\mathrm{C}^\top\mathbf{x}_\mathrm{B} + \omega_y\mathbf{y}_\mathrm{C}^\top\mathbf{z}_\mathrm{B}\right). \tag{25}$$

The body rates can now be obtained by solving the linear system of equations composed of (17), (18), and (25).

To compute the angular accelerations $\dot{\boldsymbol{\omega}}$ as functions of the flat outputs and their derivatives, we take the derivative of (17), (18), and (25) to get a similar linear system of equations as

$$\begin{aligned} &\dot{\omega}_y \left(c - \left(d_z - d_x\right)\left(\mathbf{z}_\mathrm{B}^\top\mathbf{v}\right)\right) - \dot{\omega}_z \left(d_x - d_y\right)\left(\mathbf{y}_\mathrm{B}^\top\mathbf{v}\right) \\ &\quad = \mathbf{x}_\mathrm{B}^\top\mathbf{s} - 2\dot{c}\omega_y - c\omega_x\omega_z + \mathbf{x}_\mathrm{B}^\top\boldsymbol{\xi} \end{aligned} \tag{26}$$

$$\begin{aligned} &\dot{\omega}_x \left(c + \left(d_y - d_z\right)\left(\mathbf{z}_\mathrm{B}^\top\mathbf{v}\right)\right) + \dot{\omega}_z \left(d_x - d_y\right)\left(\mathbf{x}_\mathrm{B}^\top\mathbf{v}\right) \\ &\quad = -\mathbf{y}_\mathrm{B}^\top\mathbf{s} - 2\dot{c}\omega_x + c\omega_y\omega_z - \mathbf{y}_\mathrm{B}^\top\boldsymbol{\xi} \end{aligned} \tag{27}$$

$$\begin{aligned} &-\dot{\omega}_y\mathbf{y}_\mathrm{C}^\top\mathbf{z}_\mathrm{B} + \dot{\omega}_z\|\mathbf{y}_\mathrm{C} \times \mathbf{z}_\mathrm{B}\| \\ &\quad = \ddot{\psi}\mathbf{x}_\mathrm{C}^\top\mathbf{x}_\mathrm{B} + 2\dot{\psi}\omega_z\mathbf{x}_\mathrm{C}^\top\mathbf{y}_\mathrm{B} - 2\dot{\psi}\omega_y\mathbf{x}_\mathrm{C}^\top\mathbf{z}_\mathrm{B} \\ &\qquad - \omega_x\omega_y\mathbf{y}_\mathrm{C}^\top\mathbf{y}_\mathrm{B} - \omega_x\omega_z\mathbf{y}_\mathrm{C}^\top\mathbf{z}_\mathrm{B} \end{aligned} \tag{28}$$

which we can solve for $\dot{\boldsymbol{\omega}}$ with

$$\begin{aligned} \dot{c} &= \mathbf{z}_\mathrm{B}^\top\mathbf{j} + \omega_x\left(d_y - d_z\right)\left(\mathbf{y}_\mathrm{B}^\top\mathbf{v}\right) \\ &\quad + \omega_y\left(d_z - d_x\right)\left(\mathbf{x}_\mathrm{B}^\top\mathbf{v}\right) + d_z\mathbf{z}_\mathrm{B}^\top\mathbf{a} \end{aligned} \tag{29}$$

$$\begin{aligned} \boldsymbol{\xi} &= \mathbf{R}\left(\hat{\boldsymbol{\omega}}^2\mathbf{D} + \mathbf{D}\hat{\boldsymbol{\omega}}^2 + 2\hat{\boldsymbol{\omega}}\mathbf{D}\hat{\boldsymbol{\omega}}^\top\right)\mathbf{R}^\top\mathbf{v} \\ &\quad + 2\mathbf{R}\left(\hat{\boldsymbol{\omega}}\mathbf{D} + \mathbf{D}\hat{\boldsymbol{\omega}}^\top\right)\mathbf{R}^\top\mathbf{a} + \mathbf{R}\mathbf{D}\mathbf{R}^\top\mathbf{j}. \end{aligned} \tag{30}$$

Once we know the angular accelerations, we can solve (4) for the torque inputs $\boldsymbol{\tau}$.

Note that, besides quadrotors, this proof also applies to multi-rotor vehicles with parallel rotor axes in general. More details of this proof can be found in our technical report [15].

V. Control Law

To track a reference trajectory, we use a controller consisting of feedback terms computed from tracking errors as well as feed-forward terms computed from the reference trajectory using the quadrotor's differential flatness property. Apart from special cases, the control architectures of typical quadrotors do not allow to apply the torque inputs directly. They instead provide a low-level body-rate controller, which accepts desired body rates. In order to account for this possibility, we designed our control algorithm with a classical cascaded structure, i.e., consisting of a high-level position controller and the low-level body-rate controller. The high-level position controller computes the desired orientation $\mathbf{R}_\mathrm{des}$, the collective thrust input c_cmd, the desired body rates

$\boldsymbol{\omega}_{\text{des}}$, and the desired angular accelerations $\dot{\boldsymbol{\omega}}_{\text{des}}$, which are then applied in a low-level controller (e.g. as presented in [16]). As a first step in the position controller, we compute the desired acceleration of the quadrotor's body as

$$\mathbf{a}_{\text{des}} = \mathbf{a}_{\text{fb}} + \mathbf{a}_{\text{ref}} - \mathbf{a}_{\text{rd}} + g\mathbf{z}_{\text{W}} \tag{31}$$

where $\mathbf{a}_{\text{fb}}$ are the PD feedback-control terms computed from the position and velocity control errors as

$$\mathbf{a}_{\text{fb}} = -\mathbf{K}_{\text{pos}}\left(\mathbf{p} - \mathbf{p}_{\text{ref}}\right) - \mathbf{K}_{\text{vel}}\left(\mathbf{v} - \mathbf{v}_{\text{ref}}\right) \tag{32}$$

where $\mathbf{K}_{\text{pos}}$ and $\mathbf{K}_{\text{vel}}$ are constant diagonal matrices and $\mathbf{a}_{\text{rd}} = -\mathbf{R}_{\text{ref}}\mathbf{D}\mathbf{R}_{\text{ref}}^{\top}\mathbf{v}_{\text{ref}}$ are the accelerations due to rotor drag. We compute the desired orientation $\mathbf{R}_{\text{des}}$ such that the desired acceleration $\mathbf{a}_{\text{des}}$ and the reference heading ψ_{ref} is respected as

$$\mathbf{z}_{\text{B,des}} = \frac{\mathbf{a}_{\text{des}}}{\|\mathbf{a}_{\text{des}}\|} \tag{33}$$

$$\mathbf{x}_{\text{B,des}} = \frac{\mathbf{y}_{\text{C}} \times \mathbf{z}_{\text{B,des}}}{\|\mathbf{y}_{\text{C}} \times \mathbf{z}_{\text{B,des}}\|} \tag{34}$$

$$\mathbf{y}_{\text{B,des}} = \mathbf{z}_{\text{B,des}} \times \mathbf{x}_{\text{B,des}}. \tag{35}$$

By projecting the desired accelerations onto the actual body z-axis and considering the thrust model (5), we can then compute the collective thrust input as

$$c_{\text{cmd}} = \mathbf{a}_{\text{des}}^{\top}\mathbf{z}_{\text{B}} - k_h(\mathbf{v}^{\top}(\mathbf{x}_{\text{B}} + \mathbf{y}_{\text{B}}))^2. \tag{36}$$

Similarly, we can compute the desired body rates as

$$\boldsymbol{\omega}_{\text{des}} = \boldsymbol{\omega}_{\text{fb}} + \boldsymbol{\omega}_{\text{ref}} \tag{37}$$

where $\boldsymbol{\omega}_{\text{fb}}$ are the feedback terms computed from an attitude controller (e.g. as presented in [17]) and $\boldsymbol{\omega}_{\text{ref}}$ are feed-forward terms from the reference trajectory, which are computed as described in Section IV. Finally, the desired angular accelerations are the reference angular accelerations

$$\dot{\boldsymbol{\omega}}_{\text{des}} = \dot{\boldsymbol{\omega}}_{\text{ref}} \tag{38}$$

which are computed from the reference trajectory as described in Section IV.

VI. Drag Coefficients Estimation

To apply the presented control law with inputs $[c_{\text{cmd}}, \boldsymbol{\omega}]$, we need to identify $\mathbf{D}$, and k_h, which are used to compute the reference inputs and the thrust command. If instead one is using a platform that is controlled by the inputs $[c_{\text{cmd}}, \boldsymbol{\tau}]$, $\mathbf{A}$ and $\mathbf{B}$ also need to be identified for computing the torque input. While $\mathbf{D}$ and k_h can be accurately estimated from measured accelerations and velocities through (2) and (5), the effects of $\mathbf{A}$ and $\mathbf{B}$ on the body-rate dynamics (4) are weaker and require to differentiate the gyro measurements as well as knowing the rotor speeds and rotor inertia to compute $\boldsymbol{\tau}$ and $\boldsymbol{\tau}_{\text{g}}$. Therefore, we propose to identify $\mathbf{D}$, $\mathbf{A}$, $\mathbf{B}$, and k_h by running a Nelder-Mead gradient free optimization [18] for which the quadrotor repeats a predefined trajectory in each iteration of the optimization. During this procedure, we control the quadrotor by the proposed control scheme with different drag coefficients in each iteration during which we record the absolute trajectory tracking error (39) and use it as cost for the optimization. Once the optimization has converged, we know the coefficients that reduce the trajectory tracking error the most. We found that the obtained values for $\mathbf{D}$ agree with an estimation through (2) when recording IMU measurements and ground truth velocity. This procedure has the advantage that no IMU and rotor speed measurements are required, which are both unavailable on our quadrotor platform used for the presented experiments, and the gyro measurements do not need to be differentiated. This is not the case when performing the identification through (2), (4), and (5). Also, since our method does not rely explicitly on (2), it can also capture first order approximations of non modeled effects lumped into the identified coefficients. Furthermore, our implementation allows stopping and restarting the optimization at any time, which allows changing the battery.

VII. Experiments

A. Experimental Setup

Our quadrotor platform is built from off-the-shelf components used for first-person-view racing (see Fig. 1). It features a carbon frame with stiff six inch propellers, a Raceflight Revolt flight controller, an Odroid XU4 single board computer, and a Laird RM024 radio module for receiving control commands. The platform weights $610\,\text{g}$ and has a thrust-to-weight ratio of 4. To improve its trajectory tracking accuracy we compensate the thrust commands for the varying battery voltage. All the presented flight experiments were conducted in an OptiTrack motion capture system to acquire the ground truth state of the quadrotor which is obtained at $200\,\text{Hz}$ and is used for control and evaluation of the trajectory tracking performance. Note that our control method and the rotor-drag coefficient identification also work with state estimates that are obtained differently than with a motion capture system. We compensate for an average latency of the perception and control pipeline of $32\,\text{ms}$. The high-level control runs on a laptop computer at $55\,\text{Hz}$, sending collective thrust and body rate commands to the on-board flight controller where they are tracked by a PD controller running at $4\,\text{kHz}$.

To evaluate the trajectory tracking performance and as cost for estimating the drag coefficients, we use the absolute trajectory tracking error defined as the root mean square position error

$$E_a = \sqrt{\frac{1}{N}\sum_{k=1}^{N}\left\|E_p^k\right\|^2}, \text{ where } \quad E_p^k = \mathbf{p}^{\text{k}} - \mathbf{p}_{\text{ref}}^{\text{k}} \tag{39}$$

over N control cycles of the high-level controller required to execute a given trajectory.

B. Trajectories

For identifying the rotor-drag coefficients and for demonstrating the trajectory tracking performance of the proposed controller, we let the quadrotor execute a horizontal circle trajectory and a horizontal Gerono lemniscate trajectory.

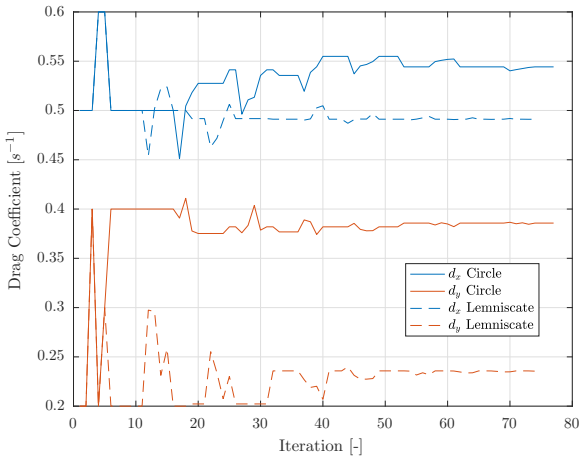


Fig. 3: The best performing drag coefficients d_x and d_y for every iteration of the identification on both the circle and the lemniscate trajectory.

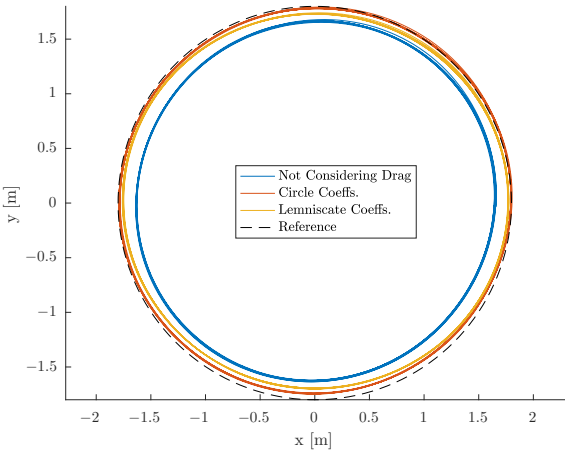


Fig. 4: Ground truth position for ten loops on the circle trajectory without considering rotor drag (solid blue), with drag coefficients estimated on the circle trajectory (solid red), and with drag coefficients estimated on the lemniscate trajectory (solid yellow) compared to the reference position (dashed black).

The circle trajectory has a radius of $1.8\,\mathrm{m}$ with a velocity of $4\,\mathrm{m\,s^{-1}}$ resulting, for the case of not considering rotor drag, in a required collective mass-normalized thrust of $c = 13.24\,\mathrm{m\,s^{-2}}$ and a maximum body rates norm of $\|\boldsymbol{\omega}\| = 85\,^\circ\,\mathrm{s^{-1}}$. Its maximum nominal velocity in the $\mathbf{x}_\mathrm{B}$ and $\mathbf{y}_\mathrm{B}$ is $4.0\,\mathrm{m\,s^{-1}}$ and $0.0\,\mathrm{m\,s^{-1}}$ in the $\mathbf{z}_\mathrm{B}$ direction. The Gerono lemniscate trajectory is defined by $\left[x(t) = 2\cos\left(\sqrt{2}t\right); y(t) = 2\sin\left(\sqrt{2}t\right)\cos\left(\sqrt{2}t\right)\right]$ with a maximum velocity of $4\,\mathrm{m\,s^{-1}}$, a maximum collective mass-normalized thrust of $c = 12.98\,\mathrm{m\,s^{-2}}$, and a maximum body rates norm of $\|\boldsymbol{\omega}\| = 136\,^\circ\,\mathrm{s^{-1}}$. Its maximum nominal velocity in the $\mathbf{x}_\mathrm{B}$ and $\mathbf{y}_\mathrm{B}$ is $2.8\,\mathrm{m\,s^{-1}}$ and $1.3\,\mathrm{m\,s^{-1}}$ in the $\mathbf{z}_\mathrm{B}$ direction for the case of not considering rotor drag.

C. Drag Coefficients Identification

To identify the drag coefficients in $\mathbf{D}$, we ran the optimization presented in Section VI multiple times on both the circle and lemniscate trajectories until it converged, i.e., until the changes of each coefficient in one iteration is below a specified threshold. We do not identify $\mathbf{A}$ and $\mathbf{B}$ since the quadrotor platform used for the presented experiments takes $[c_\mathrm{cmd}, \boldsymbol{\omega}]$ as inputs and we therefore do not need to compute the torque inputs involving $\mathbf{A}$ and $\mathbf{B}$ according to (4). Since we found that d_z and k_h only have minor effects on the trajectory tracking performance, we isolate the effects of d_x and d_y by setting $d_z = 0$ and $k_h = 0$ for the presented experiments. For each iteration of the optimization, the quadrotor flies two loops of either trajectory. The optimization typically converges after about 70 iterations, which take around $30\,\mathrm{min}$ including multiple battery swaps.

The evolution of the best performing drag coefficients is shown in Fig. 3 for every iteration of the proposed optimization. On the circle trajectory, we obtained $d_x = 0.544\,\mathrm{s^{-1}}$ and $d_y = 0.386\,\mathrm{s^{-1}}$, whereas on the lemniscate trajectory we obtained $d_x = 0.491\,\mathrm{s^{-1}}$ and $d_y = 0.236\,\mathrm{s^{-1}}$. For both trajectories, d_x is larger than d_y, which is expected because we use a quadrotor that is wider than long. The obtained drag coefficients identified on the circle are different than the ones identified on the lemniscate, which is due to the fact that the circle trajectory excites velocities in the $\mathbf{x}_\mathrm{B}$ and $\mathbf{y}_\mathrm{B}$ more than the lemniscate trajectory. We could verify this claim by running the identification on the circle trajectory with a speed of $2.8\,\mathrm{m\,s^{-1}}$, which corresponds to the maximum speeds reached in $\mathbf{x}_\mathrm{B}$ and $\mathbf{y}_\mathrm{B}$ on the lemniscate trajectory. For this speed, we obtained $d_x = 0.425\,\mathrm{s^{-1}}$, and $d_y = 0.256\,\mathrm{s^{-1}}$ on the circle trajectory, which are close to the coefficients identified on the lemniscate trajectory. Additionally, in our dynamical model, we assume the rotor drag to be independent of the thrust. This is not true in reality and therefore leads to different results of the drag coefficient estimation on different trajectories where different thrusts are applied. These reasons suggest to carefully select a trajectory for the identification, which goes towards the problem of finding the optimal trajectory for parameter estimation, which is outside the scope of this paper. In all the conducted experiments, we found that a non zero drag coefficient in the z-direction d_z does not improve the trajectory tracking performance. We found this to be true even for purely vertical trajectories with velocities of up to $2.5\,\mathrm{m\,s^{-1}}$. Furthermore, we found that an estimated $k_h = 0.009\,\mathrm{m^{-1}}$ improves the trajectory tracking performance further but by about one order of magnitude less than d_x and d_y on the considered trajectories.

D. Trajectory Tracking Performance

To demonstrate the trajectory tracking performance of the proposed control scheme, we compare the position error of our quadrotor flying the circle and the lemniscate trajectory described above for three conditions: (i) without considering rotor drag, (ii) with the drag coefficients estimated on the circle trajectory, and (iii) with the drag coefficients estimated on the lemniscate trajectory.[1] Fig. 4 shows the ground truth

[1]Video of the experiments: `https://youtu.be/VIQILwcM5PA`

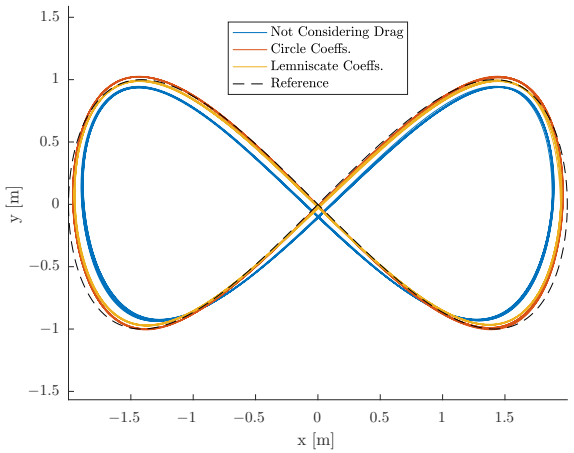


Fig. 5: Ground truth position for ten loops on the lemniscate trajectory without considering rotor drag (solid blue), with drag coefficients estimated on the circle trajectory (solid red), and with drag coefficients estimated on the lemniscate trajectory (solid yellow) compared to the reference position (dashed black).

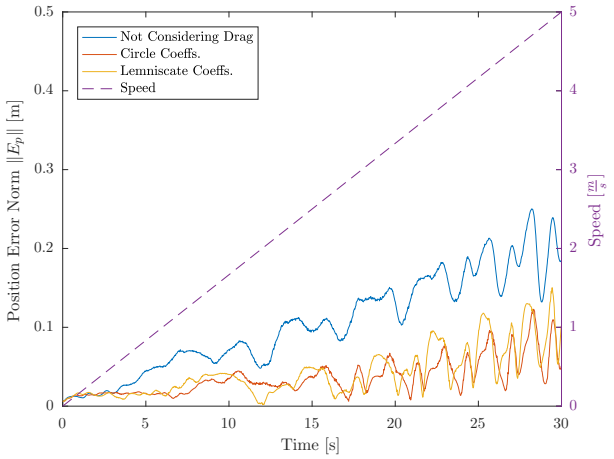


Fig. 6: Position error norm $\|E_p\|$ when ramping the speed on the circle trajectory from $0\,\mathrm{m\,s^{-1}}$ up to $5\,\mathrm{m\,s^{-1}}$ in $30\,\mathrm{s}$ without considering rotor drag (solid blue), with drag coefficients estimated on the circle trajectory (solid red), and with drag coefficients estimated on the lemniscate trajectory (solid yellow). The reference speed on the trajectory is shown in dashed purple.

and reference position when flying the circle trajectory under these three conditions. Equally, Fig. 5 shows the ground truth and reference position when flying the lemniscate trajectory under the same three conditions. The tracking performance statistics for both trajectories are summarized in Table I. From these statistics, we see that the trajectory tracking performance has improved significantly when considering rotor drag on both trajectories independently of which trajectory the rotor-drag coefficients were estimated on. This confirms that our approach is applicable to any feasible trajectory once the drag coefficients are identified, which is an advantage over methods that improve tracking performance for a specific trajectory only (e.g. [19]). With the rotor-drag coefficients estimated on the circle trajectory, we achieve almost the same performance in terms of absolute trajectory tracking error on the lemniscate trajectory as with the coefficients identified on the lemniscate trajectory but not vice versa. As discussed above, this is due to a higher excitation in body velocities on the circle trajectory which results in a better identification of the rotor-drag coefficients. This suggests to perform the rotor-drag coefficients identification on a trajectory that maximally excites the body velocities.

Since the rotor drag is a function of the velocity of the quadrotor, we show the benefits of our control approach by linearly ramping up the maximum speed on both trajectories from $0\,\mathrm{m\,s^{-1}}$ to $5\,\mathrm{m\,s^{-1}}$ in $30\,\mathrm{s}$. Fig. 6, and Fig. 7 show the position error norm and the reference speed over time until the desired maximum speed of $5\,\mathrm{m\,s^{-1}}$ is reached for the circle and the lemniscate trajectory, respectively. Both figures show that considering rotor drag does not improve trajectory tracking for small speeds below $0.5\,\mathrm{m\,s^{-1}}$ but noticeably does so for higher speeds.

An analysis of the remaining position error for the case where rotor drag is considered reveals that it strongly correlates to the applied collective thrust. In the used dynamical model of a quadrotor, we assume the rotor drag to be independent of the thrust [c.f. (2)], which is not true in reality. For the experiment in Fig. 6, the commanded mass-normalized collective thrust varies between $10\,\mathrm{m\,s^{-2}}$ and $18\,\mathrm{m\,s^{-2}}$ which clearly violates the constant thrust assumption. By considering a dependency of the rotor drag on the thrust might improve trajectory tracking even further and is subject of future work.

VIII. Comparison to Other Control Methods

In this section, we present a qualitative comparison to other quadrotor controllers that consider rotor drag effects as presented in [10], [11], [13], and [14].

None of these works show or exploit the differential flatness property of quadrotor dynamics subject to rotor drag effects. They also do not consider asymmetric vehicles where $d_x \neq d_y$ and they omit the computation of ω_z and $\dot{\omega}_z$.

In [10] and [11], the presented position controller decomposes the rotor drag force into a component that is independent of the vehicle's orientation and one along the thrust direction, which leads to an explicit expression for the

TABLE I: Maximum and standard deviation of the position error E_p as well as the absolute trajectory tracking error E_a (39) over ten loops on both the circle and the lemniscate trajectory. For each trajectory, we perform the experiment without considering drag, with the drag coefficients identified on the circle trajectory, and with the drag coefficients identified on the lemniscate trajectory.

Trajectory	Params ID	$\max(\|E_p\|)$ [cm]	$\sigma(\|E_p\|)$ [cm]	E_a [cm]
Circle	Not Cons. Drag	21.08	**2.11**	17.53
	Circle	14.54	2.63	**6.54**
	Lemniscate	**12.39**	2.53	8.16
Lemniscate	Not Cons. Drag	16.79	3.19	11.27
	Circle	10.25	2.30	5.56
	Lemniscate	**10.02**	**2.23**	**5.51**

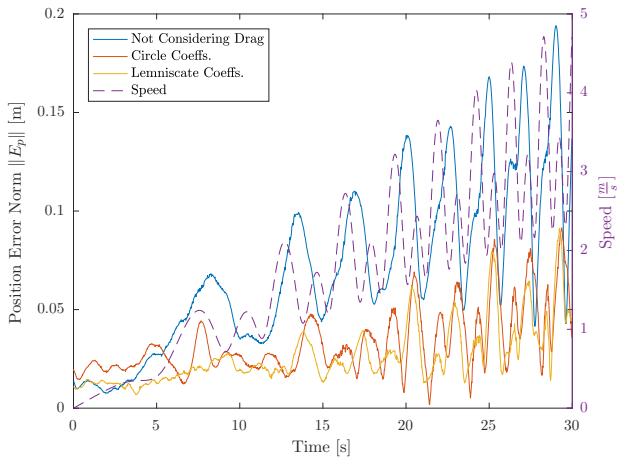


Fig. 7: Position error norm $\|E_p\|$ when ramping the maximum speed on the lemniscate trajectory from $0\,\mathrm{m\,s^{-1}}$ up to $5\,\mathrm{m\,s^{-1}}$ in $30\,\mathrm{s}$ without considering rotor drag (solid blue), with drag coefficients estimated on the circle trajectory (solid red), and with drag coefficients estimated on the lemniscate trajectory (solid yellow). The reference speed on the trajectory is shown in dashed purple.

desired thrust direction. They both neglect feed-forward on angular accelerations, which does not allow perfect trajectory tracking. As in our work, [10] models the rotor drag to be proportional to the square root of the thrust, which is proportional to the rotor speed, but then assumes the thrust to be constant for the computation of the rotor drag, whereas [11] models the rotor drag to be proportional to the thrust. Simulation results are presented in [10] while real experiments with speeds of up to $2.5\,\mathrm{m\,s^{-1}}$ were conducted in [11].

The controller in [13] considers rotor drag in the computation of the thrust command and the desired orientation but it does not use feed-forward terms on body rates and angular accelerations, which does not allow perfect trajectory tracking. In our work, we use the same thrust model but neglect its dependency on the rotor speed. In [13], also the rotor drag is modeled to depend on the rotor speed, which is physically correct but requires the rotor speeds to be measured for it to be considered in the controller. They present real experiments with speeds of up to $4.0\,\mathrm{m\,s^{-1}}$ and unlike us also show trajectory tracking improvements in vertical flight.

As in our work, [14] considers rotor drag for the computation of the desired thrust, orientation, body rates, and angular accelerations. However, their computations rely on a model where the rotor drag is proportional to the rotor thrust. Also, they neglect the snap of the trajectory and instead require the estimated acceleration and jerk, which are typically not available, for computing the desired body rates and angular accelerations. The presented results in [14] stem from real experiments with speeds of up to $1.0\,\mathrm{m\,s^{-1}}$.

IX. Conclusion

We proved that the dynamical model of a quadrotor subject to linear rotor drag effects is differentially flat. This property was exploited to compute feed-forward control terms as algebraic functions of a reference trajectory to be tracked. We presented a control policy that uses these feed-forward terms, which compensates for rotor drag effects, and therefore improves the trajectory tracking performance of a quadrotor already from speeds of $0.5\,\mathrm{m\,s^{-1}}$ onwards. The proposed control method reduces the root mean squared tracking error by $50\,\%$ independently of the executed trajectory, which we showed by evaluating the tracking performance of a circle and a lemniscate trajectory. In future work, we want to consider the dependency of the rotor drag on the applied thrust to further improve the trajectory tracking performance of quadrotors.

References

[1] M. Burri, M. Bloesch, Z. Taylor, R. Siegwart, and J. Nieto, "A framework for maximum likelihood parameter identification applied on MAVs," *J. Field Robot.*, June 2017.

[2] D. Mellinger and V. Kumar, "Minimum snap trajectory generation and control for quadrotors," in *IEEE Int. Conf. Robot. Autom. (ICRA)*, May 2011, pp. 2520–2525.

[3] J. Ferrin, R. Leishman, R. Beard, and T. McLain, "Differential flatness based control of a rotorcraft for aggressive maneuvers," in *IEEE/RSJ Int. Conf. Intell. Robot. Syst. (IROS)*, Sept. 2011.

[4] P. J. Bristeau, P. Martin, E. Salaün, and N. Petit, "The role of propeller aerodynamics in the model of a quadrotor UAV," in *IEEE Eur. Control Conf. (ECC)*, Aug. 2009, pp. 683–688.

[5] P. Martin and E. Salaün, "The true role of accelerometer feedback in quadrotor control," in *IEEE Int. Conf. Robot. Autom. (ICRA)*, 2010.

[6] R. Mahony, V. Kumar, and P. Corke, "Multirotor aerial vehicles: Modeling, estimation, and control of quadrotor," *IEEE Robot. Autom. Mag.*, vol. 19, no. 3, pp. 20–32, 2012.

[7] R. C. Leishman, J. C. Macdonald, R. W. Beard, and T. W. McLain, "Quadrotors and accelerometers: State estimation with an improved dynamic model," *Control Systems, IEEE*, vol. 34, no. 1, pp. 28–41, Feb. 2014.

[8] M. Burri, M. Dätwiler, M. W. Achtelik, and R. Siegwart, "Robust state estimation for micro aerial vehicles based on system dynamics," in *IEEE Int. Conf. Robot. Autom. (ICRA)*, 2015.

[9] M. Bangura and R. Mahony, "Thrust control for multirotor aerial vehicles," *IEEE Trans. Robot.*, vol. 33, no. 2, pp. 390–405, Apr. 2017.

[10] J.-M. Kai, G. Allibert, M.-D. Hua, and T. Hamel, "Nonlinear feedback control of quadrotors exploiting first-order drag effects," in *IFAC World Congress*, July 2017.

[11] S. Omari, M.-D. Hua, G. Ducard, and T. Hamel, "Nonlinear control of VTOL UAVs incorporating flapping dynamics," in *IEEE/RSJ Int. Conf. Intell. Robot. Syst. (IROS)*, Nov. 2013.

[12] M.-D. Hua, T. Hamel, P. Morin, and C. Samson, "Introduction to feedback control of underactuated VTOL vehicles: A review of basic control design ideas and principles," *IEEE Control Systems*, vol. 33, no. 1, pp. 61–75, Feb. 2013.

[13] J. Svacha, K. Mohta, and V. Kumar, "Improving quadrotor trajectory tracking by compensating for aerodynamic effects," in *IEEE Int. Conf. Unmanned Aircraft Syst. (ICUAS)*, June 2017.

[14] M. Bangura, "Aerodynamics and control of quadrotors," Ph.D. dissertation, The Australian National University, 2017.

[15] M. Faessler, A. Franchi, and D. Scaramuzza, "Detailed derivations of 'differential flatness of quadrotor dynamics subject to rotor drag for accurate tracking of high-speed trajectories'," 2018, arXiv.

[16] M. Faessler, D. Falanga, and D. Scaramuzza, "Thrust mixing, saturation, and body-rate control for accurate aggressive quadrotor flight," *IEEE Robot. Autom. Lett.*, vol. 2, no. 2, pp. 476–482, Apr. 2017.

[17] M. Faessler, F. Fontana, C. Forster, and D. Scaramuzza, "Automatic re-initialization and failure recovery for aggressive flight with a monocular vision-based quadrotor," in *IEEE Int. Conf. Robot. Autom. (ICRA)*, 2015, pp. 1722–1729.

[18] J. A. Nelder and R. Mead, "A simplex method for function minimization," *The Computer Journal*, vol. 7, no. 4, pp. 308–313, Jan. 1965.

[19] M. Hehn and R. D'Andrea, "A frequency domain iterative learning algorithm for high-performance, periodic quadrocopter maneuvers," *J. Mechatronics*, vol. 24, no. 8, pp. 954–965, 2014.

Detailed Derivations of *"Differential Flatness of Quadrotor Dynamics Subject to Rotor Drag for Accurate Tracking of High-Speed Trajectories"*

Matthias Faessler, Antonio Franchi, and Davide Scaramuzza

Abstract

This technical report provides detailed intermediate steps of the proof of differential flatness of quadrotor dynamics subject to rotor drag effects presented in [1]. It also shows how we handle singularities that arise from this math for certain states related to free fall of the quadrotor. Furthermore, it explains incorrectnesses in the proof of differential flatness of quadrotor dynamics *without* rotor drag presented in [2] which might be confusing when comparing the two works.

How to Cite this Work

This technical report is accompanying our IEEE Robotics and Automation Letters paper [1]. If you wish to reference this work, please cite this paper as follows:

```
@Article{Faessler18ral,
  author  = {Matthias Faessler and Antonio Franchi
             and Davide Scaramuzza},
  title   = {Differential Flatness of Quadrotor Dynamics
             Subject to Rotor Drag for Accurate,
             High-Speed Trajectory Tracking},
  journal = {{IEEE} Robot. Autom. Lett.},
  year    = 2018,
  volume  = 3,
  number  = 2,
  pages   = {620--626},
  month   = apr,
  doi     = {10.1109/LRA.2017.2776353},
  issn    = {2377-3766}
}
```

Contents

1 Math Basics **3**
1.1 Definitions and Nomenclature 3
1.2 Some Useful Identities and Derivations 4
1.3 Vector Derivatives in Different Coordinate Frames 4

2 Dynamical Model **5**

3 Proof of Differential Flatness **6**
3.1 Orientation and Thrust 6
3.2 Body Rates 7
3.3 Torque Inputs 9

4 Special Cases **11**

Appendices **14**

A Incorrectnesses in Original Differential Flatness Derivation **14**

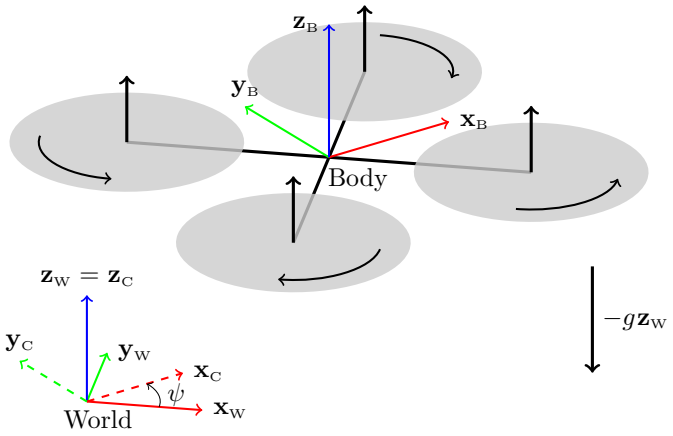


Figure 1: Schematics of the considered quadrotor model with the used coordinate systems.

1 Math Basics

1.1 Definitions and Nomenclature

In this work, we make use of a world frame W with orthonormal basis $\{\mathbf{x}_\mathrm{W}, \mathbf{y}_\mathrm{W}, \mathbf{z}_\mathrm{W}\}$ represented in *world coordinates* and a body frame B with orthonormal basis $\{\mathbf{x}_\mathrm{B}, \mathbf{y}_\mathrm{B}, \mathbf{z}_\mathrm{B}\}$ also represented in *world coordinates*. The body frame is fixed to the quadrotor with an origin coinciding with its center of mass as depicted in Fig. 1. The quadrotor is subject to a gravitational acceleration g in negative $\mathbf{z}_\mathrm{W}$ direction. We denote the position of the quadrotor's center of mass as $\mathbf{p}$, and its derivatives, velocity, acceleration, jerk, and snap as $\mathbf{v}$, $\mathbf{a}$, $\mathbf{j}$, and $\mathbf{s}$, respectively. We represent the quadrotor's orientation as a rotation matrix $\mathbf{R} = \begin{bmatrix}\mathbf{x}_\mathrm{B} & \mathbf{y}_\mathrm{B} & \mathbf{z}_\mathrm{B}\end{bmatrix}$ and its body rates (i.e., the angular velocity) as $\boldsymbol{\omega}$ represented in *body coordinates*. In this work, we often make use of a skew symmetric matrix formed from the body rates which is defined by

$$\hat{\boldsymbol{\omega}} = \begin{bmatrix} 0 & -\omega_z & \omega_y \\ \omega_z & 0 & -\omega_x \\ -\omega_y & \omega_x & 0 \end{bmatrix}. \tag{1}$$

We define a rotor drag matrix, which is a constant diagonal matrix composed of the rotor drag coefficients, as

$$\mathbf{D} = \begin{bmatrix} d_\mathrm{x} & 0 & 0 \\ 0 & d_\mathrm{y} & 0 \\ 0 & 0 & d_\mathrm{z} \end{bmatrix}. \tag{2}$$

To denote unit vectors along the coordinate axes we use

$$\mathbf{e}_{\text{x}} = \begin{bmatrix} 1 & 0 & 0 \end{bmatrix}^\top \tag{3}$$

$$\mathbf{e}_{\text{y}} = \begin{bmatrix} 0 & 1 & 0 \end{bmatrix}^\top \tag{4}$$

$$\mathbf{e}_{\text{z}} = \begin{bmatrix} 0 & 0 & 1 \end{bmatrix}^\top. \tag{5}$$

Finally, we denote quantities that can be computed from a reference trajectory as *reference values* and quantities that are computed by an outer loop feedback control law and passed to an inner loop controller as *desired values*.

1.2 Some Useful Identities and Derivations

The skew symmetric matrix $\hat{\boldsymbol{\omega}}$ has the following properties:

$$\hat{\boldsymbol{\omega}}^\top = -\hat{\boldsymbol{\omega}} \tag{6}$$

$$\hat{\boldsymbol{\omega}}^\top \cdot \mathbf{b} = -\hat{\boldsymbol{\omega}} \cdot \mathbf{b} = -\boldsymbol{\omega} \times \mathbf{b} = \mathbf{b} \times \boldsymbol{\omega} \tag{7}$$

where $\mathbf{b}$ is an arbitrary vector. The derivative of the orientation is

$$\dot{\mathbf{R}} = \mathbf{R} \cdot \hat{\boldsymbol{\omega}} \tag{8}$$

and the derivative of the norm of a vector $\mathbf{b}$ can be written as

$$\frac{d}{dt} \|\mathbf{b}\| = \frac{\mathbf{b}^\top \cdot \dot{\mathbf{b}}}{\|\mathbf{b}\|}. \tag{9}$$

Finally, in this work, we make use of the vector triple product of arbitrary vectors $\mathbf{a}$, $\mathbf{b}$, and $\mathbf{c}$:

$$\mathbf{a}^\top(\mathbf{b} \times \mathbf{c}) = -\mathbf{b}^\top(\mathbf{a} \times \mathbf{c}). \tag{10}$$

1.3 Vector Derivatives in Different Coordinate Frames

Since derivatives of vectors that are represented in different coordinate frames are important for the derivations in the proof of differential flatness of quadrotor dynamics, we introduce them here in detail. To avoid confusion in this section, unlike in the rest of this report, we use subscripts to explicitly denote what each variable depicts and in which coordinates it is represented. We denote the derivative of an arbitrary vector $\mathbf{b}$ which is then represented in a coordinate frame A as ${}_{\text{A}}(\dot{\mathbf{b}})$ and the pure element wise derivative as ${}_{\text{A}}\dot{\mathbf{b}}$.

Since the world frame W is an inertial frame, taking the derivative of a vector represented in world coordinates corresponds to taking the element wise derivative

$${}_{\text{W}}(\dot{\mathbf{b}}) = {}_{\text{W}}\dot{\mathbf{b}}. \tag{11}$$

A vector represented in world coordinates ${}_{\text{W}}\mathbf{b}$ is related to its representation in body coordinates ${}_{\text{B}}\mathbf{b}$ by a rotation $\mathbf{R}_{\text{WB}}$ that represents the orientation of the body frame B with respect to the world frame W as

$${}_{\text{W}}\mathbf{b} = \mathbf{R}_{\text{WB}} \cdot {}_{\text{B}}\mathbf{b}. \tag{12}$$

With this and (8), we can write (11) as

$$ {}_{\mathrm{W}}(\dot{\mathbf{b}}) = {}_{\mathrm{W}}\dot{\mathbf{b}} = \mathbf{R}_{\mathrm{WB}} \cdot {}_{\mathrm{B}}\dot{\mathbf{b}} + \mathbf{R}_{\mathrm{WB}} \cdot {}_{\mathrm{B}}\hat{\boldsymbol{\omega}}_{\mathrm{WB}} \cdot {}_{\mathrm{B}}\mathbf{b}. \tag{13} $$

Transforming this into body coordinates results in

$$ {}_{\mathrm{B}}(\dot{\mathbf{b}}) = \mathbf{R}_{\mathrm{WB}}^{\top} \cdot {}_{\mathrm{W}}(\dot{\mathbf{b}}) = {}_{\mathrm{B}}\dot{\mathbf{b}} + {}_{\mathrm{B}}\boldsymbol{\omega}_{\mathrm{WB}} \times {}_{\mathrm{B}}\mathbf{b}. \tag{14} $$

In this work, we often make use of derivatives of the basis vectors of the body frame $\mathbf{x}_{\mathrm{B}}$, $\mathbf{y}_{\mathrm{B}}$, and $\mathbf{z}_{\mathrm{B}}$. Since these vectors are constant when represented in body coordinates their element wise derivative in body coordinates is zero (e.g., ${}_{\mathrm{B}}\dot{\mathbf{x}}_{\mathrm{B}} = \mathbf{0}$). Therefore, we get the derivative of e.g. $\mathbf{x}_{\mathrm{B}}$ represented in world and body coordinates as

$$ {}_{\mathrm{W}}(\dot{\mathbf{x}}_{\mathrm{B}}) = \mathbf{R}_{\mathrm{WB}} \cdot {}_{\mathrm{B}}\hat{\boldsymbol{\omega}}_{\mathrm{WB}} \cdot {}_{\mathrm{B}}\mathbf{x}_{\mathrm{B}} \tag{15} $$

$$ {}_{\mathrm{B}}(\dot{\mathbf{x}}_{\mathrm{B}}) = {}_{\mathrm{B}}\hat{\boldsymbol{\omega}}_{\mathrm{WB}} \cdot {}_{\mathrm{B}}\mathbf{x}_{\mathrm{B}} = {}_{\mathrm{B}}\boldsymbol{\omega}_{\mathrm{WB}} \times {}_{\mathrm{B}}\mathbf{x}_{\mathrm{B}}. \tag{16} $$

Since we almost exclusively represent vectors in world coordinates and the element wise derivative of the basis vectors are zero, we will write the derivative of a basis vector represented in world coordinates as $\dot{\mathbf{x}}_{\mathrm{B}}$ instead of ${}_{\mathrm{W}}(\dot{\mathbf{x}}_{\mathrm{B}})$, as it is done in [1], for clarity in the remainder of this report.

Note that a confusion of derivatives of vectors represented in world coordinates or in body coordinates led to mistakes in [2], which we describe in more detail in Appendix A.

2 Dynamical Model

We consider the dynamical model of a quadrotor with rotor drag developed in [3] with no wind, stiff propellers, and no dependence of the rotor drag on the thrust. According to this model, the dynamics of the position $\mathbf{p}$, velocity $\mathbf{v}$, orientation $\mathbf{R}$, and body rates $\boldsymbol{\omega}$ can be written as

$$ \dot{\mathbf{p}} = \mathbf{v} \tag{17} $$

$$ \dot{\mathbf{v}} = -g\mathbf{z}_{\mathrm{W}} + c\mathbf{z}_{\mathrm{B}} - \mathbf{R}\mathbf{D}\mathbf{R}^{\top}\mathbf{v} \tag{18} $$

$$ \dot{\mathbf{R}} = \mathbf{R}\hat{\boldsymbol{\omega}} \tag{19} $$

$$ \dot{\boldsymbol{\omega}} = \mathbf{J}^{-1}\left(\boldsymbol{\tau} - \boldsymbol{\omega} \times \mathbf{J}\boldsymbol{\omega} - \boldsymbol{\tau}_{\mathrm{g}} - \mathbf{A}\mathbf{R}^{\top}\mathbf{v} - \mathbf{B}\boldsymbol{\omega}\right) \tag{20} $$

where c is the mass-normalized collective thrust, $\mathbf{D} = \mathrm{diag}\left(d_{\mathrm{x}}, d_{\mathrm{y}}, d_{\mathrm{z}}\right)$ is a constant diagonal matrix formed by the mass-normalized rotor-drag coefficients, $\hat{\boldsymbol{\omega}}$ is a skew-symmetric matrix formed from $\boldsymbol{\omega}$, $\mathbf{J}$ is the quadrotor's inertia matrix, $\boldsymbol{\tau}$ is the three dimensional torque input, $\boldsymbol{\tau}_{\mathrm{g}}$ are gyroscopic torques from the propellers, and $\mathbf{A}$ and $\mathbf{B}$ are constant matrices. For the derivations and more details about these terms, please refer to [3]. In this work, we adopt the thrust model presented in [4]

$$ c = c_{\mathrm{cmd}} + k_h v_h^2 \tag{21} $$

where c_{cmd} is the commanded collective thrust input, k_h is a constant, and $v_h = \mathbf{v}^\top(\mathbf{x}_\text{B} + \mathbf{y}_\text{B})$. The term $k_h v_h^2$ acts as a quadratic velocity-dependent input disturbance which adds up to the input c_{cmd}. The additional linear velocity-dependent disturbance in the $\mathbf{z}_\text{B}$ direction of the thrust model in [4] is lumped by d_z directly in (18) by neglecting its dependency on the rotor speeds. Note that this dynamical model of a quadrotor is a generalization of the common model found, e.g., in [2], in which the linear rotor drag components are typically neglected, i.e., $\mathbf{D}$, $\mathbf{A}$ and $\mathbf{B}$ are considered null matrices.

3 Proof of Differential Flatness

In this section, we show that the extended dynamical model of a quadrotor subject to rotor drag (17)-(20) with four inputs is differentially flat, like the model with neglected drag [2]. In fact, we shall show that the states $[\mathbf{p}, \mathbf{v}, \mathbf{R}, \boldsymbol{\omega}]$ and the inputs $[c_{\text{cmd}}, \boldsymbol{\tau}]$ can be written as algebraic functions of four selected flat outputs and a finite number of their derivatives. Equally to [2], we choose the flat outputs to be the quadrotor's position $\mathbf{p}$ and its heading ψ.

3.1 Orientation and Thrust

To show that the orientation $\mathbf{R}$ and the collective thrust c are functions of the flat outputs, we reformulate (18) as

$$c\mathbf{z}_\text{B} - \mathbf{R}\mathbf{D}\mathbf{R}^\top\mathbf{v} = \mathbf{a} + g\mathbf{z}_\text{W} \tag{22}$$

$$c\mathbf{z}_\text{B} - \begin{bmatrix}\mathbf{x}_\text{B} & \mathbf{y}_\text{B} & \mathbf{z}_\text{B}\end{bmatrix}\begin{bmatrix}d_x & 0 & 0\\ 0 & d_y & 0\\ 0 & 0 & d_z\end{bmatrix}\begin{bmatrix}\mathbf{x}_\text{B}^\top\\ \mathbf{y}_\text{B}^\top\\ \mathbf{z}_\text{B}^\top\end{bmatrix}\cdot\mathbf{v} = \mathbf{a} + g\mathbf{z}_\text{W} \tag{23}$$

$$c\mathbf{z}_\text{B} - (d_x\mathbf{x}_\text{B}^\top\mathbf{v})\,\mathbf{x}_\text{B} - (d_y\mathbf{y}_\text{B}^\top\mathbf{v})\,\mathbf{y}_\text{B} - (d_z\mathbf{z}_\text{B}^\top\mathbf{v})\,\mathbf{z}_\text{B} = \mathbf{a} + g\mathbf{z}_\text{W}. \tag{24}$$

Left-multiply (24) by $\mathbf{x}_\text{B}^\top$

$$-d_x\mathbf{x}_\text{B}^\top\mathbf{v} = \mathbf{x}_\text{B}^\top(\mathbf{a} + g\mathbf{z}_\text{W}) \tag{25}$$

$$\mathbf{x}_\text{B}^\top(\mathbf{a} + g\mathbf{z}_\text{W} + d_x\mathbf{v}) = 0. \tag{26}$$

Left-multiply (24) by $\mathbf{y}_\text{B}^\top$

$$-d_y\mathbf{y}_\text{B}^\top\mathbf{v} = \mathbf{y}_\text{B}^\top(\mathbf{a} + g\mathbf{z}_\text{W}) \tag{27}$$

$$\mathbf{y}_\text{B}^\top(\mathbf{a} + g\mathbf{z}_\text{W} + d_y\mathbf{v}) = 0. \tag{28}$$

To form an orthonormal basis we additionally require

$$\mathbf{x}_\text{B}^\top\mathbf{x}_\text{B} = 1 \tag{29}$$

$$\mathbf{y}_\text{B}^\top\mathbf{y}_\text{B} = 1 \tag{30}$$

$$\mathbf{x}_\text{B}^\top\mathbf{y}_\text{B} = 0. \tag{31}$$

To enforce a reference heading ψ, we constrain the projection of the $\mathbf{x}_\mathrm{B}$ axis into the $\mathbf{x}_\mathrm{W} - \mathbf{y}_\mathrm{W}$ plane to be collinear with $\mathbf{x}_\mathrm{C}$ (c.f. Fig 1), where

$$\mathbf{x}_\mathrm{C} = \begin{bmatrix}\cos(\psi) & \sin(\psi) & 0\end{bmatrix}^\top \tag{32}$$

$$\mathbf{y}_\mathrm{C} = \begin{bmatrix}-\sin(\psi) & \cos(\psi) & 0\end{bmatrix}^\top. \tag{33}$$

From these constraints we can construct $\mathbf{R}$ with

$$\mathbf{x}_\mathrm{B} = \frac{\mathbf{y}_\mathrm{C} \times \boldsymbol{\alpha}}{\|\mathbf{y}_\mathrm{C} \times \boldsymbol{\alpha}\|} \tag{34}$$

$$\mathbf{y}_\mathrm{B} = \frac{\boldsymbol{\beta} \times \mathbf{x}_\mathrm{B}}{\|\boldsymbol{\beta} \times \mathbf{x}_\mathrm{B}\|} \tag{35}$$

$$\mathbf{z}_\mathrm{B} = \mathbf{x}_\mathrm{B} \times \mathbf{y}_\mathrm{B} \tag{36}$$

as

$$\mathbf{R} = \begin{bmatrix}\mathbf{x}_\mathrm{B} & \mathbf{y}_\mathrm{B} & \mathbf{z}_\mathrm{B}\end{bmatrix} \tag{37}$$

where

$$\boldsymbol{\alpha} = \mathbf{a} + g\mathbf{z}_\mathrm{W} + d_\mathrm{x}\mathbf{v} \tag{38}$$

$$\boldsymbol{\beta} = \mathbf{a} + g\mathbf{z}_\mathrm{W} + d_\mathrm{y}\mathbf{v}. \tag{39}$$

One can verify that these vectors are of unit length, perpendicular to each other, and satisfy the constraints (26) - (33). To get the thrust input, we left-multiply (24) by $\mathbf{z}_\mathrm{B}^\top$

$$c - d_\mathrm{z}\mathbf{z}_\mathrm{B}^\top\mathbf{v} = \mathbf{z}_\mathrm{B}^\top(\mathbf{a} + g\mathbf{z}_\mathrm{W}) \tag{40}$$

$$c = \mathbf{z}_\mathrm{B}^\top(\mathbf{a} + g\mathbf{z}_\mathrm{W} + d_\mathrm{z}\mathbf{v}). \tag{41}$$

Then the collective thrust input can be computed as a function of c, $\mathbf{R}$, and the flat outputs, according to the thrust model (21) as

$$c_\mathrm{cmd} = c - k_h(\mathbf{v}^\top(\mathbf{x}_\mathrm{B} + \mathbf{y}_\mathrm{B}))^2. \tag{42}$$

3.2 Body Rates

To show that the body rates $\boldsymbol{\omega}$ are functions of the flat outputs and their derivatives, we take the derivative of (18)

$$\mathbf{j} = \dot{c}\mathbf{z}_\mathrm{B} + c\mathbf{R}\hat{\boldsymbol{\omega}}\mathbf{e}_z - \mathbf{R}\left(\left(\hat{\boldsymbol{\omega}}\mathbf{D} + \mathbf{D}\hat{\boldsymbol{\omega}}^\top\right)\mathbf{R}^\top\mathbf{v} + \mathbf{D}\mathbf{R}^\top\mathbf{a}\right). \tag{43}$$

Left multiply (43) by $\mathbf{x}_\mathrm{B}^\top$

$$\mathbf{x}_\mathrm{B}^\top\mathbf{j} = c\omega_y - \omega_z\left(d_\mathrm{x} - d_\mathrm{y}\right)\left(\mathbf{y}_\mathrm{B}^\top\mathbf{v}\right) - \omega_y\left(d_\mathrm{z} - d_\mathrm{x}\right)\left(\mathbf{z}_\mathrm{B}^\top\mathbf{v}\right) - d_\mathrm{x}\mathbf{x}_\mathrm{B}^\top\mathbf{a}. \tag{44}$$

Left multiply (43) by $\mathbf{y}_\mathrm{B}^\top$

$$\mathbf{y}_\mathrm{B}^\top\mathbf{j} = -c\omega_x - \omega_z\left(d_\mathrm{x} - d_\mathrm{y}\right)\left(\mathbf{x}_\mathrm{B}^\top\mathbf{v}\right) - \omega_x\left(d_\mathrm{y} - d_\mathrm{z}\right)\left(\mathbf{z}_\mathrm{B}^\top\mathbf{v}\right) - d_\mathrm{y}\mathbf{y}_\mathrm{B}^\top\mathbf{a}. \tag{45}$$

By projecting (19) along the $\mathbf{y}_{\text{B}}$ we get

$$\mathbf{y}_{\text{B}}^{\top}\dot{\mathbf{R}} = \mathbf{y}_{\text{B}}^{\top}\mathbf{R}\hat{\boldsymbol{\omega}} \tag{46}$$

$$\omega_z = \mathbf{y}_{\text{B}}^{\top}\dot{\mathbf{x}}_{\text{B}}. \tag{47}$$

Since $\mathbf{x}_{\text{B}}$ is perpendicular to $\mathbf{y}_{\text{C}}$ and $\mathbf{z}_{\text{B}}$, we can write

$$\mathbf{x}_{\text{B}} = \frac{\tilde{\mathbf{x}}_{\text{B}}}{\|\tilde{\mathbf{x}}_{\text{B}}\|}, \text{ with } \quad \tilde{\mathbf{x}}_{\text{B}} = \mathbf{y}_{\text{C}} \times \mathbf{z}_{\text{B}}. \tag{48}$$

Taking its derivative as the general derivative of a normalized vector, we get

$$\dot{\mathbf{x}}_{\text{B}} = \frac{\dot{\tilde{\mathbf{x}}}_{\text{B}}}{\|\tilde{\mathbf{x}}_{\text{B}}\|} - \tilde{\mathbf{x}}_{\text{B}}\frac{\tilde{\mathbf{x}}_{\text{B}}^{\top}\dot{\tilde{\mathbf{x}}}_{\text{B}}}{\|\tilde{\mathbf{x}}_{\text{B}}\|^3}. \tag{49}$$

Since $\tilde{\mathbf{x}}_{\text{B}}$ is collinear to $\mathbf{x}_{\text{B}}$ and therefore perpendicular to $\mathbf{y}_{\text{B}}$, we can write (47) as

$$\omega_z = \mathbf{y}_{\text{B}}^{\top}\frac{\dot{\tilde{\mathbf{x}}}_{\text{B}}}{\|\tilde{\mathbf{x}}_{\text{B}}\|}. \tag{50}$$

The derivative of $\tilde{\mathbf{x}}_{\text{B}}$ can be computed as

$$\dot{\tilde{\mathbf{x}}}_{\text{B}} = \dot{\mathbf{y}}_{\text{C}} \times \mathbf{z}_{\text{B}} + \mathbf{y}_{\text{C}} \times \dot{\mathbf{z}}_{\text{B}} \tag{51}$$

where, using (15),

$$\dot{\mathbf{y}}_{\text{C}} = \mathbf{R}_{\text{WC}}\left(\dot{\psi}\mathbf{e}_{\text{z}} \times \mathbf{e}_{\text{y}}\right) \tag{52}$$

$$= \begin{bmatrix}\mathbf{x}_{\text{C}} & \mathbf{y}_{\text{C}} & \mathbf{z}_{\text{C}}\end{bmatrix}\left(-\dot{\psi}\mathbf{e}_{\text{x}}\right) \tag{53}$$

$$= -\dot{\psi}\mathbf{x}_{\text{C}} \tag{54}$$

and

$$\dot{\mathbf{z}}_{\text{B}} = \mathbf{R}\hat{\boldsymbol{\omega}}\mathbf{e}_{\text{z}} \tag{55}$$

$$= \mathbf{R}\begin{bmatrix}\omega_y \\ -\omega_x \\ 0\end{bmatrix} \tag{56}$$

$$= \omega_y\mathbf{x}_{\text{B}} - \omega_x\mathbf{y}_{\text{B}} \tag{57}$$

and therefore

$$\dot{\tilde{\mathbf{x}}}_{\text{B}} = -\dot{\psi}\mathbf{x}_{\text{C}} \times \mathbf{z}_{\text{B}} + \omega_y\mathbf{y}_{\text{C}} \times \mathbf{x}_{\text{B}} - \omega_x\mathbf{y}_{\text{C}} \times \mathbf{y}_{\text{B}}. \tag{58}$$

From this and (50) and using the property in (10), we then get

$$\omega_z = \mathbf{y}_{\mathrm{B}}^{\top} \frac{\dot{\tilde{\mathbf{x}}}_{\mathrm{B}}}{\|\tilde{\mathbf{x}}_{\mathrm{B}}\|} \tag{59}$$

$$= \frac{1}{\|\tilde{\mathbf{x}}_{\mathrm{B}}\|} \left(-\dot{\psi} \mathbf{y}_{\mathrm{B}}^{\top} \left(\mathbf{x}_{\mathrm{C}} \times \mathbf{z}_{\mathrm{B}} \right) + \omega_y \mathbf{y}_{\mathrm{B}}^{\top} \left(\mathbf{y}_{\mathrm{C}} \times \mathbf{x}_{\mathrm{B}} \right) \right) \tag{60}$$

$$= \frac{1}{\|\tilde{\mathbf{x}}_{\mathrm{B}}\|} \left(\dot{\psi} \mathbf{x}_{\mathrm{C}}^{\top} \left(\mathbf{y}_{\mathrm{B}} \times \mathbf{z}_{\mathrm{B}} \right) - \omega_y \mathbf{y}_{\mathrm{C}}^{\top} \left(\mathbf{y}_{\mathrm{B}} \times \mathbf{x}_{\mathrm{B}} \right) \right) \tag{61}$$

$$= \frac{1}{\|\tilde{\mathbf{x}}_{\mathrm{B}}\|} \left(\dot{\psi} \mathbf{x}_{\mathrm{C}}^{\top} \mathbf{x}_{\mathrm{B}} + \omega_y \mathbf{y}_{\mathrm{C}}^{\top} \mathbf{z}_{\mathrm{B}} \right). \tag{62}$$

The body rates can then be computed from a linear system of equations composed of (44), (45), and (62)

$$\omega_y \left(c - (d_z - d_x) \left(\mathbf{z}_{\mathrm{B}}^{\top} \mathbf{v} \right) \right) - \omega_z \left(d_x - d_y \right) \left(\mathbf{y}_{\mathrm{B}}^{\top} \mathbf{v} \right) = \mathbf{x}_{\mathrm{B}}^{\top} \mathbf{j} + d_x \mathbf{x}_{\mathrm{B}}^{\top} \mathbf{a} \tag{63}$$

$$\omega_x \left(c + (d_y - d_z) \left(\mathbf{z}_{\mathrm{B}}^{\top} \mathbf{v} \right) \right) + \omega_z \left(d_x - d_y \right) \left(\mathbf{x}_{\mathrm{B}}^{\top} \mathbf{v} \right) = -\mathbf{y}_{\mathrm{B}}^{\top} \mathbf{j} - d_y \mathbf{y}_{\mathrm{B}}^{\top} \mathbf{a} \tag{64}$$

$$-\omega_y \mathbf{y}_{\mathrm{C}}^{\top} \mathbf{z}_{\mathrm{B}} + \omega_z \left\| \mathbf{y}_{\mathrm{C}} \times \mathbf{z}_{\mathrm{B}} \right\| = \dot{\psi} \mathbf{x}_{\mathrm{C}}^{\top} \mathbf{x}_{\mathrm{B}} \tag{65}$$

as

$$\omega_x = \frac{-\mathcal{B}_1 \mathcal{C}_2 \mathcal{D}_3 + \mathcal{B}_1 \mathcal{C}_3 \mathcal{D}_2 - \mathcal{B}_3 \mathcal{C}_1 \mathcal{D}_2 + \mathcal{B}_3 \mathcal{C}_2 \mathcal{D}_1}{\mathcal{A}_2 \left(\mathcal{B}_1 \mathcal{C}_3 - \mathcal{B}_3 \mathcal{C}_1 \right)} \tag{66}$$

$$\omega_y = \frac{-\mathcal{C}_1 \mathcal{D}_3 + \mathcal{C}_3 \mathcal{D}_1}{\mathcal{B}_1 \mathcal{C}_3 - \mathcal{B}_3 \mathcal{C}_1} \tag{67}$$

$$\omega_z = \frac{\mathcal{B}_1 \mathcal{D}_3 - \mathcal{B}_3 \mathcal{D}_1}{\mathcal{B}_1 \mathcal{C}_3 - \mathcal{B}_3 \mathcal{C}_1} \tag{68}$$

where

$$\mathcal{B}_1 = c - (d_z - d_x) \left(\mathbf{z}_{\mathrm{B}}^{\top} \mathbf{v} \right) \tag{69}$$

$$\mathcal{C}_1 = -\left(d_x - d_y \right) \left(\mathbf{y}_{\mathrm{B}}^{\top} \mathbf{v} \right) \tag{70}$$

$$\mathcal{D}_1 = \mathbf{x}_{\mathrm{B}}^{\top} \mathbf{j} + d_x \mathbf{x}_{\mathrm{B}}^{\top} \mathbf{a} \tag{71}$$

$$\mathcal{A}_2 = c + (d_y - d_z) \left(\mathbf{z}_{\mathrm{B}}^{\top} \mathbf{v} \right) \tag{72}$$

$$\mathcal{C}_2 = \left(d_x - d_y \right) \left(\mathbf{x}_{\mathrm{B}}^{\top} \mathbf{v} \right) \tag{73}$$

$$\mathcal{D}_2 = -\mathbf{y}_{\mathrm{B}}^{\top} \mathbf{j} - d_y \mathbf{y}_{\mathrm{B}}^{\top} \mathbf{a} \tag{74}$$

$$\mathcal{B}_3 = -\mathbf{y}_{\mathrm{C}}^{\top} \mathbf{z}_{\mathrm{B}} \tag{75}$$

$$\mathcal{C}_3 = \left\| \mathbf{y}_{\mathrm{C}} \times \mathbf{z}_{\mathrm{B}} \right\| \tag{76}$$

$$\mathcal{D}_3 = \dot{\psi} \mathbf{x}_{\mathrm{C}}^{\top} \mathbf{x}_{\mathrm{B}}. \tag{77}$$

3.3 Torque Inputs

To show that the angular accelerations $\dot{\boldsymbol{\omega}}$ are functions of the flat outputs and their derivatives, we take the derivative of (43)

$$\mathbf{s} = \ddot{c} \mathbf{z}_{\mathrm{B}} + 2\dot{c} \mathbf{R} \hat{\boldsymbol{\omega}} \mathbf{e}_z + c \left(\mathbf{R} \hat{\boldsymbol{\omega}}^2 \mathbf{e}_z + \mathbf{R} \dot{\hat{\boldsymbol{\omega}}} \mathbf{e}_z \right) - \mathbf{R} \left(\dot{\hat{\boldsymbol{\omega}}} \mathbf{D} + \mathbf{D} \dot{\hat{\boldsymbol{\omega}}}^{\top} \right) \mathbf{R}^{\top} \mathbf{v} - \boldsymbol{\xi} \tag{78}$$

where

$$\boldsymbol{\xi} = \mathbf{R}(\hat{\boldsymbol{\omega}}^2\mathbf{D} + \mathbf{D}\hat{\boldsymbol{\omega}}^2 + 2\hat{\boldsymbol{\omega}}\mathbf{D}\hat{\boldsymbol{\omega}}^\top)\,\mathbf{R}^\top\mathbf{v} + 2\mathbf{R}(\hat{\boldsymbol{\omega}}\mathbf{D} + \mathbf{D}\hat{\boldsymbol{\omega}}^\top)\,\mathbf{R}^\top\mathbf{a} + \mathbf{R}\mathbf{D}\mathbf{R}^\top\mathbf{j}. \quad (79)$$

Left multiplying (78) by $\mathbf{x}_{\mathrm{B}}^\top$ and rearranging terms

$$\dot{\omega}_y\mathcal{B}_1 + \dot{\omega}_z\mathcal{C}_1 = \mathbf{x}_{\mathrm{B}}^\top\mathbf{s} - 2\dot{c}\omega_y - c\omega_x\omega_z + \mathbf{x}_{\mathrm{B}}^\top\boldsymbol{\xi}. \quad (80)$$

Left multiplying (78) by $\mathbf{y}_{\mathrm{B}}^\top$ and rearranging terms

$$\dot{\omega}_x\mathcal{A}_2 + \dot{\omega}_z\mathcal{C}_2 = -\mathbf{y}_{\mathrm{B}}^\top\mathbf{s} - 2\dot{c}\omega_x + c\omega_y\omega_z - \mathbf{y}_{\mathrm{B}}^\top\boldsymbol{\xi}. \quad (81)$$

We get a third constraint for the angular accelerations by differentiating (65) and using (48) as

$$\begin{aligned} &-\dot{\omega}_y\mathbf{y}_{\mathrm{C}}^\top\mathbf{z}_{\mathrm{B}} - \omega_y\dot{\mathbf{y}}_{\mathrm{C}}^\top\mathbf{z}_{\mathrm{B}} - \omega_y\mathbf{y}_{\mathrm{C}}^\top\dot{\mathbf{z}}_{\mathrm{B}} + \dot{\omega}_z\left\|\mathbf{y}_{\mathrm{C}}\times\mathbf{z}_{\mathrm{B}}\right\| + \omega_z\frac{\tilde{\mathbf{x}}_{\mathrm{B}}^\top\dot{\tilde{\mathbf{x}}}_{\mathrm{B}}}{\|\tilde{\mathbf{x}}_{\mathrm{B}}\|} \\ &= \ddot{\psi}\mathbf{x}_{\mathrm{C}}^\top\mathbf{x}_{\mathrm{B}} + \dot{\psi}\dot{\mathbf{x}}_{\mathrm{C}}^\top\mathbf{x}_{\mathrm{B}} + \dot{\psi}\mathbf{x}_{\mathrm{C}}^\top\dot{\mathbf{x}}_{\mathrm{B}} \end{aligned} \quad (82)$$

which can be simplified to

$$\begin{aligned} -\dot{\omega}_y\mathbf{y}_{\mathrm{C}}^\top\mathbf{z}_{\mathrm{B}} + \dot{\omega}_z\left\|\mathbf{y}_{\mathrm{C}}\times\mathbf{z}_{\mathrm{B}}\right\| = \ddot{\psi}\mathbf{x}_{\mathrm{C}}^\top\mathbf{x}_{\mathrm{B}} + 2\dot{\psi}\omega_z\mathbf{x}_{\mathrm{C}}^\top\mathbf{y}_{\mathrm{B}} - 2\dot{\psi}\omega_y\mathbf{x}_{\mathrm{C}}^\top\mathbf{z}_{\mathrm{B}} \\ - \omega_x\omega_y\mathbf{y}_{\mathrm{C}}^\top\mathbf{y}_{\mathrm{B}} - \omega_x\omega_z\mathbf{y}_{\mathrm{C}}^\top\mathbf{z}_{\mathrm{B}} \end{aligned} \quad (83)$$

by using the following derivations:
From (54) we get

$$-\omega_y\dot{\mathbf{y}}_{\mathrm{C}}^\top\mathbf{z}_{\mathrm{B}} = \dot{\psi}\omega_y\mathbf{x}_{\mathrm{C}}^\top\mathbf{z}_{\mathrm{B}}. \quad (84)$$

From(57) and the fact that $\mathbf{y}_{\mathrm{C}}^\top\mathbf{x}_{\mathrm{B}} = 0$, we get

$$-\omega_y\mathbf{y}_{\mathrm{C}}^\top\dot{\mathbf{z}}_{\mathrm{B}} = \omega_x\omega_y\mathbf{y}_{\mathrm{C}}^\top\mathbf{y}_{\mathrm{B}}. \quad (85)$$

From (48) and using (10) and (58) we get

$$\omega_z\frac{\tilde{\mathbf{x}}_{\mathrm{B}}^\top\dot{\tilde{\mathbf{x}}}_{\mathrm{B}}}{\|\tilde{\mathbf{x}}_{\mathrm{B}}\|} = \omega_z\mathbf{x}_{\mathrm{B}}^\top\dot{\tilde{\mathbf{x}}}_{\mathrm{B}} \quad (86)$$

$$= \omega_z\mathbf{x}_{\mathrm{B}}^\top\left(-\dot{\psi}\mathbf{x}_{\mathrm{C}}\times\mathbf{z}_{\mathrm{B}} + \omega_y\mathbf{y}_{\mathrm{C}}\times\mathbf{x}_{\mathrm{B}} - \omega_x\mathbf{y}_{\mathrm{C}}\times\mathbf{y}_{\mathrm{B}}\right) \quad (87)$$

$$= \omega_z\left(-\dot{\psi}\mathbf{x}_{\mathrm{B}}^\top(\mathbf{x}_{\mathrm{C}}\times\mathbf{z}_{\mathrm{B}}) - \omega_x\mathbf{x}_{\mathrm{B}}^\top(\mathbf{y}_{\mathrm{C}}\times\mathbf{y}_{\mathrm{B}})\right) \quad (88)$$

$$= \omega_z\left(\dot{\psi}\mathbf{x}_{\mathrm{C}}^\top(\mathbf{x}_{\mathrm{B}}\times\mathbf{z}_{\mathrm{B}}) + \omega_x\mathbf{y}_{\mathrm{C}}^\top(\mathbf{x}_{\mathrm{B}}\times\mathbf{y}_{\mathrm{B}})\right) \quad (89)$$

$$= \omega_z\left(-\dot{\psi}\mathbf{x}_{\mathrm{C}}^\top\mathbf{y}_{\mathrm{B}} + \omega_x\mathbf{y}_{\mathrm{C}}^\top\mathbf{z}_{\mathrm{B}}\right). \quad (90)$$

Similarly to (54), we can derive

$$\dot{\mathbf{x}}_{\mathrm{C}} = \mathbf{R}_{\mathrm{WC}}\left(\dot{\psi}\mathbf{e}_{\mathrm{z}}\times\mathbf{e}_{\mathrm{x}}\right) \quad (91)$$

$$= \begin{bmatrix}\mathbf{x}_{\mathrm{C}} & \mathbf{y}_{\mathrm{C}} & \mathbf{z}_{\mathrm{C}}\end{bmatrix}\left(\dot{\psi}\mathbf{e}_{\mathrm{y}}\right) \quad (92)$$

$$= \dot{\psi}\mathbf{y}_{\mathrm{C}} \quad (93)$$

and with this and the fact that $\mathbf{y}_{\mathrm{C}}^{\top}\mathbf{x}_{\mathrm{B}} = 0$

$$\dot{\psi}\dot{\mathbf{x}}_{\mathrm{C}}^{\top}\mathbf{x}_{\mathrm{B}} = \dot{\psi}^2\mathbf{y}_{\mathrm{C}}^{\top}\mathbf{x}_{\mathrm{B}} = \mathbf{0}. \tag{94}$$

And finally, similarly to (57), we get

$$\dot{\mathbf{x}}_{\mathrm{B}} = \mathbf{R}\hat{\boldsymbol{\omega}}\mathbf{e}_{\mathrm{x}} \tag{95}$$

$$= \mathbf{R}\begin{bmatrix} 0 \\ \omega_z \\ -\omega_y \end{bmatrix} \tag{96}$$

$$= \omega_z\mathbf{y}_{\mathrm{B}} - \omega_y\mathbf{z}_{\mathrm{B}} \tag{97}$$

which leads to

$$\dot{\psi}\mathbf{x}_{\mathrm{C}}^{\top}\dot{\mathbf{x}}_{\mathrm{B}} = \dot{\psi}\omega_z\mathbf{x}_{\mathrm{C}}^{\top}\mathbf{y}_{\mathrm{B}} - \dot{\psi}\omega_y\mathbf{x}_{\mathrm{C}}^{\top}\mathbf{z}_{\mathrm{B}}. \tag{98}$$

The derivative of the thrust can be obtained by left multiplying (43) by $\mathbf{z}_{\mathrm{B}}^{\top}$

$$\dot{c} = \mathbf{z}_{\mathrm{B}}^{\top}\mathbf{j} + \omega_x\left(d_{\mathrm{y}} - d_z\right)\left(\mathbf{y}_{\mathrm{B}}^{\top}\mathbf{v}\right) + \omega_y\left(d_z - d_{\mathrm{x}}\right)\left(\mathbf{x}_{\mathrm{B}}^{\top}\mathbf{v}\right) + d_z\mathbf{z}_{\mathrm{B}}^{\top}\mathbf{a}. \tag{99}$$

The angular accelerations can now be computed from a linear system of equations composed of (80), (81), and (83)

$$\dot{\omega}_y\mathcal{B}_1 + \dot{\omega}_z\mathcal{C}_1 = \mathcal{E}_1 \tag{100}$$

$$\dot{\omega}_x\mathcal{A}_2 + \dot{\omega}_z\mathcal{C}_2 = \mathcal{E}_2 \tag{101}$$

$$\dot{\omega}_y\mathcal{B}_3 + \dot{\omega}_z\mathcal{C}_3 = \mathcal{E}_3 \tag{102}$$

as

$$\dot{\omega}_x = \frac{-\mathcal{B}_1\mathcal{C}_2\mathcal{E}_3 + \mathcal{B}_1\mathcal{C}_3\mathcal{E}_2 - \mathcal{B}_3\mathcal{C}_1\mathcal{E}_2 + \mathcal{B}_3\mathcal{C}_2\mathcal{E}_1}{\mathcal{A}_2\left(\mathcal{B}_1\mathcal{C}_3 - \mathcal{B}_3\mathcal{C}_1\right)} \tag{103}$$

$$\dot{\omega}_y = \frac{-\mathcal{C}_1\mathcal{E}_3 + \mathcal{C}_3\mathcal{E}_1}{\mathcal{B}_1\mathcal{C}_3 - \mathcal{B}_3\mathcal{C}_1} \tag{104}$$

$$\dot{\omega}_z = \frac{\mathcal{B}_1\mathcal{E}_3 - \mathcal{B}_3\mathcal{E}_1}{\mathcal{B}_1\mathcal{C}_3 - \mathcal{B}_3\mathcal{C}_1} \tag{105}$$

where

$$\mathcal{E}_1 = \mathbf{x}_{\mathrm{B}}^{\top}\mathbf{s} - 2\dot{c}\omega_y - c\omega_x\omega_z + \mathbf{x}_{\mathrm{B}}^{\top}\boldsymbol{\xi} \tag{106}$$

$$\mathcal{E}_2 = -\mathbf{y}_{\mathrm{B}}^{\top}\mathbf{s} - 2\dot{c}\omega_x + c\omega_y\omega_z - \mathbf{y}_{\mathrm{B}}^{\top}\boldsymbol{\xi} \tag{107}$$

$$\mathcal{E}_3 = \ddot{\psi}\mathbf{x}_{\mathrm{C}}^{\top}\mathbf{x}_{\mathrm{B}} + 2\dot{\psi}\omega_z\mathbf{x}_{\mathrm{C}}^{\top}\mathbf{y}_{\mathrm{B}} - 2\dot{\psi}\omega_y\mathbf{x}_{\mathrm{C}}^{\top}\mathbf{z}_{\mathrm{B}} - \omega_x\omega_y\mathbf{y}_{\mathrm{C}}^{\top}\mathbf{y}_{\mathrm{B}} - \omega_x\omega_z\mathbf{y}_{\mathrm{C}}^{\top}\mathbf{z}_{\mathrm{B}}. \tag{108}$$

The torque inputs can finally be computed from (20).

4 Special Cases

In this section, we present some practical workarounds for some special cases where the presented math is not valid. These workarounds typically only work if we can assume that these special cases only occur for very short durations at a time.

Case - $\mathbf{y}_\mathrm{C} \times \boldsymbol{\alpha} = \mathbf{0}$: This case occurs if either $\mathbf{y}_\mathrm{C}$ is aligned with $\boldsymbol{\alpha}$ (defined in (38)) or $\boldsymbol{\alpha} = \mathbf{0}$. In this case, any $\mathbf{x}_\mathrm{B}$ that is perpendicular to $\mathbf{y}_\mathrm{C}$ satisfies the constraint (26). To overcome this ambiguity, we compute $\mathbf{x}_\mathrm{B}$ by projecting the estimated body x-axis into the $\mathbf{x}_\mathrm{C} - \mathbf{z}_\mathrm{C}$ plane and normalizing it as

$$\mathbf{x}_\mathrm{B} = \frac{\mathbf{x}_{\mathrm{B,est}} - \left(\mathbf{x}_{\mathrm{B,est}}^\top \mathbf{y}_\mathrm{C}\right) \mathbf{y}_\mathrm{C}}{\left\| \mathbf{x}_{\mathrm{B,est}} - \left(\mathbf{x}_{\mathrm{B,est}}^\top \mathbf{y}_\mathrm{C}\right) \mathbf{y}_\mathrm{C} \right\|}. \tag{109}$$

If the obtained $\left\| \mathbf{x}_{\mathrm{B,est}} - \left(\mathbf{x}_{\mathrm{B,est}}^\top \mathbf{y}_\mathrm{C}\right) \mathbf{y}_\mathrm{C} \right\| = \mathbf{0}$, we set $\mathbf{x}_\mathrm{B} = \mathbf{x}_\mathrm{C}$. Note that this might lead to jumps in the desired orientation. By assuming that this special case only occurs for a short duration it might be better to just remember the last desired orientation that was computed before the special case occurred.

Case - $\boldsymbol{\beta} \times \mathbf{x}_\mathrm{B} = \mathbf{0}$: This case occurs if either $\mathbf{x}_\mathrm{B}$ is aligned with $\boldsymbol{\beta}$ (defined in (39)) or $\boldsymbol{\beta} = \mathbf{0}$. In this case, any $\mathbf{y}_\mathrm{B}$ that is perpendicular to $\mathbf{x}_\mathrm{B}$ satisfies the constraint (54). To overcome this ambiguity, we compute $\mathbf{y}_\mathrm{B}$ by the cross product of the estimated body z-axis $\mathbf{z}_{\mathrm{B,est}}$ and $\mathbf{x}_\mathrm{B}$ and normalizing it as

$$\mathbf{y}_\mathrm{B} = \frac{\mathbf{z}_{\mathrm{B,est}} \times \mathbf{x}_\mathrm{B}}{\left\| \mathbf{z}_{\mathrm{B,est}} \times \mathbf{x}_\mathrm{B} \right\|}. \tag{110}$$

If the obtained $\left\| \mathbf{z}_{\mathrm{B,est}} \times \mathbf{x}_\mathrm{B} \right\| = \mathbf{0}$, we set $\mathbf{y}_\mathrm{B} = \mathbf{y}_\mathrm{C}$. Note that this might lead to jumps in the desired orientation. By assuming that this special case only occurs for a short duration it might be better to just remember the last desired orientation that was computed before the special case occurred.

Case - Inverted Flight where $\mathbf{z}_\mathrm{W}^\top \boldsymbol{\alpha} < 0$: In the case where $\mathbf{z}_\mathrm{W}^\top \boldsymbol{\alpha} < 0$, (34) leads to a body x-axis $\mathbf{x}_\mathrm{B}$ which has a projection into the $\mathbf{x}_\mathrm{W} - \mathbf{y}_\mathrm{W}$ plane that points into the $-\mathbf{x}_\mathrm{C}$ direction. It is still collinear to $\mathbf{x}_\mathrm{C}$ but this causes the actual heading to be off by 180° from the reference heading ψ_ref. Enforcing the reference heading during inverted flight by changing the sign of the desired $\mathbf{x}_\mathrm{B}$ axis might lead to a jump in the desired orientation. However, to the best of our knowledge, it is not possible to prevent jumps in the orientation for any trajectory. For example, when performing a vertical loop where parts of it are flown upside down, we end up with a continuous orientation of the quadrotor for a reference heading $\psi_\mathrm{ref} = 0°$ when allowing the quadrotor to have its actual heading 180° off as long as it flies upside down. When doing the same with a reference heading $\psi_\mathrm{ref} = 90°$, we do not end up with a continuous orientation of the quadrotor when applying the same method. In this particular case, changing the sign of $\mathbf{x}_\mathrm{B}$ when the quadrotor is inverted, would lead to a continuous orientation over the entire loop. In summary, the presented computation of the desired orientation is not well suited for inverted flights, which require special considerations.

Case - $\mathcal{A}_2 = 0$ or $(\mathcal{B}_1\mathcal{C}_3 - \mathcal{B}_3\mathcal{C}_1) = 0$: The solutions of the body rates (66)-(68) and angular accelerations (103)-(105) are obtained by divisions where the

denominator is composed of coefficients as defined in (69)-(77). These denominator can become zero which makes the body rates and angular accelerations undefined. Similarly to $\boldsymbol{\alpha} = \mathbf{0}$ and $\boldsymbol{\beta} = \mathbf{0}$, this is the case where the quadrotor is executing ballistic trajectories. In such cases we set $\boldsymbol{\omega} = \mathbf{0}$ and $\dot{\boldsymbol{\omega}} = \mathbf{0}$.

Appendices

A Incorrectnesses in Original Differential Flatness Derivation

The work presented in [1] extends the work of [2], which can be considered the first paper that proves differential flatness for quadrotors without considering rotor drag. However, we would like to point out two incorrectnesses found in [2] that might be confusing when comparing it to our derivations. For this, we use red color to refer to equations in [2]. Note that in this work we are using a different index convention, i.e., we denote the rotation rates of e.g. B with respect to W as $\boldsymbol{\omega}_{\mathrm{WB}}$ whereas it is denoted as $\boldsymbol{\omega}_{\mathrm{BW}}$ in [2] but in this section, we adopt their convention when referring to their equations.

The first incorrectness in [2] is due to a confusion of the representation of vectors in world or body coordinates (see Section 1.3 for details). In equation (7) the derivative of equation (3) is computed as

$$m\dot{\mathbf{a}} = \dot{u}_1 \mathbf{z}_{\mathrm{B}} + \boldsymbol{\omega}_{\mathrm{BW}} \times u_1 \mathbf{z}_{\mathrm{B}}. \tag{111}$$

However, equation (3) including $\mathbf{z}_{\mathrm{B}}$ is represented in world coordinates. By taking its derivative, we get

$$\begin{aligned} m\dot{\mathbf{a}} &= \dot{u}_1 \mathbf{z}_{\mathrm{B}} + u_1 \dot{\mathbf{z}}_{\mathrm{B}} && (112)\\ &= \dot{u}_1 \mathbf{z}_{\mathrm{B}} + u_1 \mathbf{R}\hat{\boldsymbol{\omega}}\mathbf{e}_{\mathrm{z}}. && (113) \end{aligned}$$

The fallacy in (111) is that $\dot{\mathbf{z}}_{\mathrm{B}}$ is computed as if $\mathbf{z}_{\mathrm{B}}$ was represented in body coordinates (c.f. (16)) but it is represented in world coordinates and hence its derivative is $\dot{\mathbf{z}}_{\mathrm{B}} = \mathbf{R}\hat{\boldsymbol{\omega}}\mathbf{e}_{\mathrm{z}}$, (c.f. (15)). However, by chance, the correct roll and pitch rates are obtained in [2] since the projections of $\boldsymbol{\omega}_{\mathrm{BW}} \times \mathbf{z}_{\mathrm{B}}$ and $\mathbf{R}\hat{\boldsymbol{\omega}}\mathbf{e}_{\mathrm{z}}$ onto the $\mathbf{x}_{\mathrm{B}}$ and $\mathbf{y}_{\mathrm{B}}$ axes are equal. Note that when taking the second derivative of equation (3) as done in [2] and computing the angular accelerations from that, unlike for the body rates, would not result in correct values anymore.

The second incorrectness in [2] in the same section in the computation of the third component of the body rates. It is stated that *"the third component r is found by simply writing $\boldsymbol{\omega}_{\mathrm{BW}} = \boldsymbol{\omega}_{\mathrm{BC}} + \boldsymbol{\omega}_{\mathrm{CW}}$ and observing that $\boldsymbol{\omega}_{\mathrm{BC}}$ has no $\mathbf{z}_{\mathrm{B}}$ component"*, which is not correct, i.e., generally $\boldsymbol{\omega}_{\mathrm{BC}} \cdot \mathbf{z}_{\mathrm{B}} \neq 0$. Based on this incorrect assumption, the third component of the body rates is then computed as

$$r = \boldsymbol{\omega}_{\mathrm{CW}} \cdot \mathbf{z}_{\mathrm{B}} = \dot{\psi} \mathbf{z}_{\mathrm{W}} \cdot \mathbf{z}_{\mathrm{B}} \tag{114}$$

but for

$$\boldsymbol{\omega}_{\mathrm{BW}} = \boldsymbol{\omega}_{\mathrm{BC}} + \boldsymbol{\omega}_{\mathrm{CW}} \tag{115}$$

to hold, all vectors must be expressed in the same coordinate frame, which in this case has to be the B frame since the body rates $\boldsymbol{\omega}_{\mathrm{BW}}$ are expressed

in body coordinates. Conversely, $\boldsymbol{\omega}_{\mathrm{cw}} = \dot{\psi}\mathbf{z}_{\mathrm{w}}$ as used in (114) is only valid if $\boldsymbol{\omega}_{\mathrm{cw}}$ was expressed in world coordinates, which is not the case. Similarly, the angular accelerations are computed incorrectly. The necessary third constraint for computing the correct body rates is (47).

References

[1] M. Faessler, A. Franchi, and D. Scaramuzza, "Differential flatness of quadrotor dynamics subject to rotor drag for accurate tracking of high-speed trajectories," *IEEE Robot. Autom. Lett.*, vol. 3, no. 2, pp. 620–626, Apr. 2018.

[2] D. Mellinger and V. Kumar, "Minimum snap trajectory generation and control for quadrotors," in *IEEE Int. Conf. Robot. Autom. (ICRA)*, May 2011, pp. 2520–2525.

[3] J.-M. Kai, G. Allibert, M.-D. Hua, and T. Hamel, "Nonlinear feedback control of quadrotors exploiting first-order drag effects," in *IFAC World Congress*, vol. 50, no. 1, July 2017, pp. 8189–8195.

[4] J. Svacha, K. Mohta, and V. Kumar, "Improving quadrotor trajectory tracking by compensating for aerodynamic effects," in *IEEE Int. Conf. Unmanned Aircraft Syst. (ICUAS)*, June 2017, pp. 860–866.